



RESEARCH ARTICLE

Evaluation of extreme precipitation over Southeast Asia in the Coupled Model Intercomparison Project Phase 5 regional climate model results and HighResMIP global climate models

Mugni Hadi Hariadi^{1,2,3}  | Gerard van der Schrier¹ | Gert-Jan Steeneveld² | Dian Nur Ratri³ | Ardhasena Sopaheluwakan³  | Albert Klein Tank^{2,4} | Edvin Aldrian⁵ | Dodo Gunawan³ | Marie-Pierre Moine⁶ | Alessio Bellucci⁷ | Retish Senan⁸ | Etienne Tourigny⁹ | Dian Ariyani Putrasahan¹⁰ | Utoyo Aji Linarka⁵

¹Royal Netherlands Meteorological Institute (KNMI), De Bilt, The Netherlands

²Meteorology and Air Quality (MAQ) Section, Wageningen University, Wageningen, The Netherlands

³Indonesian Agency for Meteorology, Climatology and Geophysics (BMKG), Jakarta, Indonesia

⁴Met Office Hadley Centre for Climate Science and Services, Exeter, UK

⁵National Research and Innovation Agency (BRIN), Jakarta, Indonesia

⁶Centre Européen de Recherche et de Formation Avancée en Calcul Scientifique (CERFACS), Toulouse, France

⁷Istituto di Scienze dell'Atmosfera e del Clima (CNR-ISAC), Consiglio Nazionale delle Ricerche, Bologna, Italy

⁸European Centre for Medium Range Weather Forecasts (ECMWF), Reading, UK

⁹Barcelona Supercomputing Centre (BSC), Barcelona, Spain

¹⁰Max Planck Institute for Meteorology (MPI-M), Hamburg, Germany

Correspondence

Mugni Hadi Hariadi, Royal Netherlands Meteorological Institute (KNMI), Utrechtseweg 297, De Bilt 3731 GA, The Netherlands.

Email: mugni.hariadi@knmi.nl; mugni.hariadi@bmkg.go.id; mugnihadi@gmail.com

Funding information

Indonesia Endowment Fund for Education (LPDP), Grant/Award Number: S-353/LPDP.3/2019; Royal Netherlands Embassy; European Union's Horizon 2020, Grant/Award Numbers: 748750, 824084, 641727

Abstract

Modelling rainfall extremes and dry periods over the Southeast Asia (SEA) region is challenging due to the characteristics of the region, which consists of the Maritime Continent and a mountainous region; it also experiences monsoonal conditions, as it is located between the Asian summer monsoon and the Australian summer monsoon. Representing rainfall extremes is important for flood and drought assessments in the region. This paper evaluates extreme rainfall climatic indices from regional climate models from CORDEX Southeast Asia and compares them with the results of high-resolution global climate models with a comparable spatial resolution from the HighResMIP experiment. Observations indicate a high intensity of rainfall over areas affected by tropical cyclones and long consecutive dry day periods over some areas in Indochina and the southern end of Indonesia. In the model simulations, we find that both coupled and sea surface temperature-forced

This is an open access article under the terms of the [Creative Commons Attribution-NonCommercial](https://creativecommons.org/licenses/by-nc/4.0/) License, which permits use, distribution and reproduction in any medium, provided the original work is properly cited and is not used for commercial purposes.

© 2022 The Authors. *International Journal of Climatology* published by John Wiley & Sons Ltd on behalf of Royal Meteorological Society.

HighResMIP model experiments are more similar to the observations than CORDEX model results. However, the models produce a poorer simulation of precipitation intensity-related indices due to model biases in the rainfall intensity. This bias is higher in CORDEX than in HighResMIP and is evident in both the low- and high-resolution HighResMIP model versions. The comparable performances of HighResSST (atmosphere-only runs) and Hist-1950 (coupled ocean-atmosphere runs) demonstrate the accuracy of the ocean model. Comparable performances were also found for the two different resolutions of HighResMIP, suggesting that there is no improvement in the performance of the high-resolution HighResMIP model compared to the low-resolution HighResMIP model.

KEYWORDS

CDD, climate index, CORDEX, CWD, extreme precipitation, GCM, HighResMIP, Indonesia, R10mm, R195pTOT, R20mm, RCM, Rx1day, Rx5day, SDII, Southeast Asia

1 | INTRODUCTION

Precipitation plays a crucial role in flooding, droughts, and the water supply used for consumption and sanitation (e.g., see Lavers *et al.*, 2021). Kim *et al.* (2019) stated that changes in precipitation could have a more direct negative impact on civilisation than most other meteorological factors. As many socioeconomic losses are linked to extreme precipitation events (WMO, 2021), understanding the magnitude and frequency of precipitation, for both the present and future climate, is of immense importance to society. The Intergovernmental Panel on Climate Change (IPCC) Working Group I indicated that extreme precipitation is projected to intensify in the future under a warming climate (IPCC, 2021). Recent studies have indicated that anthropogenic forcing has increased the drought risk over Southeast Asia (SEA; see the formal definition in section 2) by reducing precipitation and enhancing evapotranspiration (Zhang *et al.*, 2021).

The SEA region is exposed to several types of precipitation-related hazards. Around 24 and 62% of the population live in areas that are exposed to flooding and droughts, respectively (ESCAP, UN, 2020). During the monsoon season, extreme precipitation often causes a series of floods and landslide events, like the large-scale flooding of early 2021 in Jakarta during the peak of the monsoon season; 1,300 people were evacuated (Davies, 2021). Similarly, the high-precipitation amounts associated with the cyclones in Vietnam during October 2020 caused severe floods. This was a one-in-80-year event (Luu *et al.*, 2021). Worldwide, US\$115 billion in economic losses were caused by floods from 1970 to 2019, and the second-most expensive event occurred in Thailand in 2011 (US\$45.46 billion) (WMO, 2021). Contrasting with the excessive precipitation events are the

periods with extremely low levels of precipitation; during the 2018 El Niño event, the Indonesian government declared an emergency drought alert status for seven provinces (IFRC, 2019).

In SEA, heavy precipitation events occur mostly in the monsoon season. The monsoon season in SEA is a transition from the Asian summer monsoon to the Australian summer monsoon (Wang, 2006); it follows the movement of the Intertropical Convergence Zone (ITCZ). Both the monsoon season and the dry season are affected by the conditions of the El Niño–Southern Oscillation (ENSO) (Aldrian and Susanto, 2003). In addition, some areas in SEA experience extreme precipitation due to tropical cyclone events. For example, high-category tropical cyclones in the Bay of Bengal usually occur around April and May and lead to extreme precipitation in Myanmar (Li *et al.*, 2013), and tropical cyclones in the South China Sea bring extreme precipitation to the Philippines and Vietnam (Nguyen-Thi *et al.*, 2012; Corporal-Lodangco and Leslie, 2017).

Agriculture is a sector that is heavily affected by climatic extremes. A sustainable and secure food supply strongly depends on natural resources. The IPCC climatic scenarios demonstrate an increasing trend in the frequency of extreme climatic events (IPCC, 2021). The increasing frequency and intensity of extreme weather due to climate change will have a devastating effect on food security (FAO, 2021). Some of the impacts of precipitation-related climatic extremes on sectors like agriculture are captured in specific climate indices (Moura Cardoso do Vale *et al.*, 2020). Over the last decade, the joint World Meteorological Organization (WMO) Commission for Climatology and World Climate Research Programme (WCRP) Expert Team on Climate Change Detection and Indices (ETCCDI) has put forward

a set of climate indices that provide a comprehensive overview of precipitation and temperature information, with a focus on extremes (Karl *et al.*, 1999; Klein Tank *et al.*, 2009). A selection of these indices will be used in this study.

A decrease in the abundance of rainy days in Jakarta over the period from 1866 to 2010 has been observed (Siswanto *et al.*, 2016). However, the frequency of daily rainfall exceeding 50 and 100 mm has significantly increased, and so has the daily intensity of extreme rainfall (Siswanto *et al.*, 2016). In addition, Tangang *et al.* (2018) studied multimodel simulations of the Southeast Asia Regional Climate Downscaling/Coordinated Regional Climate Downscaling Experiment (SEACLID/CORDEX-SEA) (<http://www.ukm.edu.my/seaclid-cordex>). They found that under a 2°C global warming scenario in the near future, northern Myanmar will experience more change and more climate change impacts than other areas in SEA. This is shown by the increase in the number of annual consecutive dry days (CDD), the number of days for which the rainfall is at least 50 mm (R50mm), and the maximum daily rainfall (RX1day) over the area. Meanwhile, drier conditions will be found over Indonesia and higher extreme rainfall will be found over most of Indochina (Tangang *et al.*, 2018).

By utilizing the same regional climate model (RCM) output as Tangang *et al.* (2018) and Supari *et al.* (2020) showed that under extreme (RCP8.5) and medium (RCP4.5) climate change scenarios, the annual total rainfall will decrease by 30 and 20%, respectively, for most areas in SEA by the end of the 21st century. Additionally, there are, respectively, 60 and 30% increases in the CDD values. Moreover, Amnuaylojaroen and Chanvichit (2019) found that in the near future, the projected decrease of daily precipitation amounts and the projected increase in temperature will create favourable conditions for droughts. However, according to a crop water need analysis, the SEA area will remain water-rich for agricultural purposes and the region will remain suitable for agriculture (Amnuaylojaroen and Chanvichit, 2019). Furthermore, Amnuaylojaroen (2021) found that the increase in the simple precipitation intensity index (SDII) will be followed by a decline in the number of annual consecutive dry days (CWD) over Thailand for the period from 2020 to 2029 compared to the period from 1990 to 1999.

The ability of the climate models to simulate precipitation systems often depends on their grid spacing and parameterization of physical processes such as deep convection (Rauscher *et al.*, 2010). SEA has unique physiogeographical characteristics that make it challenging to assess the future climate impact using coarsely spaced models (Ul Hasson *et al.*, 2016). It is important to be confident that models can realistically represent extreme

precipitation over the historical period before using them for climate change impact assessments.

In this study, we evaluate how well models can simulate extreme rainfall-related climate indices. More precisely, we investigate whether the latest model experiment of the High-Resolution Model Intercomparison Project (HighResMIP) outperforms the downscaled results of the previous model experiment, Coupled Model Intercomparison Project Phase 5 (CMIP5). Hariadi *et al.* (2021) found that the HighResMIP models better represent the monsoon onset and cumulative rainfall compared to the CORDEX models for SEA. While this previous study focused on the onset and characteristics of the rainy season (Hariadi *et al.*, 2021), the current study compares these two sets of experiments with observations of extreme precipitation.

A list and descriptions of the rainfall-related climate indices used in this study are given in section 2, along with a description of the study area and the statistical methods used to assess the models' performance. In section 3, we present the observed spatial distributions of the climate indices in SEA. Furthermore, we present the performances of the models in terms of how well they simulate the climate indices. Section 4 discusses the similarities of the three gridded observational datasets that are used to determine the climate indices. We also discuss the performance of the models for a number of climate indices. In the last section, we draw conclusions from our findings.

2 | MATERIALS AND METHODS

2.1 | Description of the study area

The Southeast Asia (SEA) region is located from 12.5°S–24.5°N and 92.5°–142.5°E. This region contains Vietnam, Cambodia, Laos, Thailand, Myanmar, Malaysia, and Indonesia. The rainfall in this region is dominated by the monsoon season (Hamada *et al.*, 2002; Aldrian and Susanto, 2003; Moron *et al.*, 2009). The monsoon season starts in May for north SEA and November for south SEA (Hariadi *et al.*, 2021). SEA has one of the longest monsoon seasons in the Asian region; the monsoon season ranges from 120 to 160 days for large parts of SEA (Misra and DiNapoli, 2014). Based on the annual rainfall pattern, Aldrian and Susanto (2003) divided Indonesia into three rainfall regions: the semimonsoonal region, monsoonal region, and antimonsoonal region. The ITCZ crosses the equatorial region between 10°N and 5°S twice, which means that this region has two peaks of the monsoon season; one peak occurs during boreal spring and one peak occurs in autumn. This

region is called the semimonsoonal region (Aldrian and Susanto, 2003). Every year, the monsoonal region in Indonesia experiences two phases of the monsoon season; the wet phase coincides with the presence of the ITCZ and occurs from November to March, and the dry phase occurs when a dry southeasterly wind blows from Australia from May to September. This region is located from 5°S to the south. On the contrary, the antimonsoonal region experiences a wet phase during boreal summer from May to September. This region is located over part of Sulawesi, the Moluccas, and Papua (5°S–2°N and 120°–135°E). Chang *et al.* (2005) stated that the topography of the Moluccas shelters the region from the northeast monsoon winds during boreal winter. On the contrary, during boreal summer, the topography causes the orographic uplift of southeasterly monsoon winds. The extreme rainfall in SEA is associated with the monsoonal summer season. The characteristics of extreme rainfall over SEA regions such as Indochina (You and Ting, 2021), Thailand (Limsakul and Singhruck, 2016), and Borneo (Supari *et al.*, 2016) have been explored in previous studies.

In addition, some areas in SEA are also affected by tropical cyclones, which lead to high extreme precipitation. Myanmar is affected by tropical cyclones originating in the Bay of Bengal. Tropical cyclones occur in this region with a high frequency in October and November. Stronger tropical cyclones (category 4 or above) tend to occur in April and May (Li *et al.*, 2013). Meanwhile, in Vietnam, tropical cyclones occur from July to November. The maximum rainfall contribution from the tropical cyclones to the total rainfall occurs from July to September for northern Vietnam, while for central Vietnam, this occurs in October and November (Nguyen-Thi *et al.*, 2012). In the Philippines, tropical cyclones occur in two periods. The first period is from January to May, but in the second period (June–December), the frequency of these events is more pronounced (Corporal-Lodangco and Leslie, 2017).

Furthermore, Räsänen *et al.* (2016) found that over Indochina, most of the extreme events (wet and dry) occur during ENSO events, especially during the period from March to May. Meanwhile, Supari *et al.* (2018) found that over Indonesia, the ENSO impact is prominent from June to August and September to November. Extreme events are also magnified by the equatorial wave (Ferrett *et al.*, 2020; Lubis and Respati, 2021) and Madden–Julian oscillation (MJO) conditions (Muhammad *et al.*, 2021). Lubis and Respati (2021) found that the probability of extreme rainfall events over Java increases by up to 60% during the active phases of Kelvin waves. Another study by Muhammad *et al.* (2021) showed that the active phase of the MJO increases the probability of extreme precipitation events over the eastern part of Indonesia by up

to 50%, and this increase is even higher (up to 70%) over the western and central parts of Indonesia.

2.2 | Data

2.2.1 | Observations

In SEA, the development of a comprehensive dataset based on in situ surface observations of daily precipitation amounts is challenging because of the limited density of gauges and the limited long-term availability of rainfall time series (Van den Besselaar *et al.*, 2017; Singh and Xiaosheng, 2019). Similar to the method of Hariadi *et al.* (2021), three gridded daily observational datasets are combined to provide the observed rainfall and an uncertainty estimate. The first dataset is the Southeast Asia Observation (SA-OBS) dataset. SA-OBS is a daily high-resolution land-only observational gridded precipitation and temperature dataset covering the SEA region (Van den Besselaar *et al.*, 2017). This dataset is based on the observation data collected for the South Asian Climate Assessment and Dataset (SACA&D) (Van Den Besselaar *et al.*, 2015; Marjuki *et al.*, 2016). The second dataset is the Asian Precipitation Highly Resolved Observational Data Integration toward Evaluation of Water Resources (APHRODITE) dataset (Yatagai *et al.*, 2012). This dataset is based on rain gauge observations across Asia. The third dataset is the Climate Hazards Group Infrared Precipitation with Stations v2.0 (CHIRPS) dataset (Funk *et al.*, 2015). This dataset is based on rain gauge data collected from Food and Agriculture Organization (FAO) and Global Historical Climate Network (GHCN), together with cold cloud duration information from Climate Prediction Center (CPC) and the National Oceanic and Atmospheric Administration's (NOAA) National Climate Data Center (NCDC).

2.2.2 | Model results

Our study utilizes two datasets of climate model results. The first dataset consists of results from the Coupled Model Intercomparison Project. This study uses the downscaled version of the CMIP5 results from the Coordinated Downscaling Experiment (CORDEX) SEA simulations. Six global climate models are used. The Centre National de Recherches Météorologiques (CNRM), Commonwealth Science and Industrial Research Organisation (CSIRO), European Community Earth-System (EC-Earth), and Max Planck Institute (MPI) models were downscaled using the RegCM4 model (Giorgi *et al.*, 2012) from CORDEX SEA (Ngo-Duc *et al.*, 2017; Supari

TABLE 1 Description of the models

Model	CORDEX	LR HighResSST	HR HighResSST	LR Hist-1950	HR Hist-1950
CMCC-CM2		1° × 1°, native atmosphere, regular grid 1 member	25 km, native atmosphere, regular grid 1 member	1° × 1°, native atmosphere, regular grid 1 member	25 km, native atmosphere, regular grid 1 member
CNRM5 (CORDEX) CNRM-CM6-1 (HighResMIP)	25 km resolution 1 member	250 km regridded from T1271 1 member	50 km regridded from T3591 1 member	250 km regridded from T1271 1 member	50 km regridded from T3591 1 member
CSIROMk36	25 km resolution 1 member				
EC-Earth (CORDEX) EC-Earth3 (HighResMIP)	25 km resolution 1 member	100 km grid T255 3 members (physics version)	50 km grid T511 3 members (physics version)	100 km grid T255 3 members (physics version)	50 km grid T511 3 members (physics version)
ECMWF-IFS		1° × 1° regridded from Tco199 8 members (realization)	0.5° × 0.5° regridded from Tco399 4 members (realization)	1° × 1° regridded from Tco199 8 members (realization)	0.5° × 0.5° regridded from Tco399 6 members (realization)
GFDL	25 km resolution 1 member				
HadGEM2-AO (CORDEX) HadGEM3-GC31 (HighResMIP)	25 km resolution 1 member	250 km grid N96 5 members (initialisation)	50 km grid N512 3 members (initialisation)	250 km grid N96 8 members (initialisation)	50 km grid N512 2 members (initialisation)
MPI-ESM (CORDEX) MPI-ESM1-2 (HighResMIP)	25 km resolution 1 member	100 km spectral T127 1 member	50 km spectral T255 1 member	100 km spectral T127 1 member	50 km spectral T255 1 member

Note: The first column shows, for each model, the horizontal resolution of the global model used in the resolution of the regional model from CORDEX, for which it provided lateral boundaries. The second, third, fourth, and fifth columns specify the global resolution and the number of available members of the ensemble for historically forced low-resolution (LR) atmosphere-only simulations (HighResSST) and their high-resolution (HR) equivalents, and also for ocean-atmosphere coupled low-resolution (LR) simulations using initial conditions from 1950 (Hist-1950) and their high-resolution (HR) equivalents, respectively.

et al., 2020; Tangang *et al.*, 2020). The HadGEM model was downscaled using the regional Weather Research and Forecasting (WRF3.5) model (Skamarock *et al.*, 2008) from the Asia-Pacific Economic Cooperation Climate Centre (Yang, 2012). We will refer to this model generation as CORDEX.

The second set of models comes from the High-Resolution Model Intercomparison Project (HighResMIP) (Haarsma *et al.*, 2016). These models have a spatial resolution comparable to that of the CORDEX dataset and are available from the H2020-founded Primavera project (Roberts *et al.*, 2020). This dataset contains two experiments at two resolutions. The first HighResMIP experiment is the historically forced atmosphere run for the period from 1950 to 2014 (HighResSST). This experiment used the daily 0.25° HadISST2-based dataset for the Sea Surface Temperature (SST) and sea-ice forcing. The second HighResMIP

experiment contains coupled historic runs for the period from 1950 to 2014 (Hist-1950). We use high-resolution and low-resolution datasets from both experiments. The six models that we use from HighResMIP are EC-Earth (Haarsma *et al.*, 2020), MPI (Müller *et al.*, 2018), HadGEM (Roberts *et al.*, 2019), CMCC (Cherchi *et al.*, 2019), CNRM (Voltaire *et al.*, 2019), and ECMWF (Roberts *et al.*, 2018).

We used bilinear interpolation to interpolate the model and observation datasets to a uniform grid resolution; the reference resolution is 0.25°. Due to the limitations of the models that are available from CORDEX and HighResMIP, in this study, only four models are available for both model generations; these models are CNRM, EC-Earth, HadGEM, and MPI. CSIRO and GFDL are only available for CORDEX, and CMCC and ECMWF are only available for HighResMIP. Table 1 summarizes the resolutions of the available models.

TABLE 2 List of rainfall-related extreme climate indices computed in this study

Index ID	Index name	Index definition	Unit
CDD	Maximum dry spell length	The largest number of consecutive days on which rainfall is less than 1 mm	day
CDD5D ^a	Number of CDDs >5 days	The number of CDD periods with more than 5 days per time period	<i>n</i>
CWD	Maximum wet spell length	The largest number of consecutive days on which rainfall is at least 1 mm	day
CDW5D ^a	Number of CWDs >5 days	The number of CWD periods with more than 5 days per time period	<i>n</i>
R10mm	Number of heavy rainfall days	The number of days on which rainfall is at least 10 mm	day
R20mm	Number of very heavy rainfall days	The number of days on which rainfall is at least 20 mm	day
Rx1day	Maximum daily rainfall	The highest 1-day precipitation amount	mm
Rx5day	Maximum 5-day rainfall	The highest 5-day precipitation amount	mm
R5day50mm ^a	Number of 5-day heavy precipitation periods	The number of 5 day periods with precipitation totals greater than 50 mm	<i>n</i>
R95pTOT	Precipitation percentage due to R95p days	The ratio of the cumulative rainfall on wet days with RR > RR95percentile to the total rainfall	%
SDII	Simple daily intensity index per time period	The ratio of the annual total rainfall to the number of wet days	mm·day ⁻¹

Note: The indices are calculated annually.

^aNot derived from the ETCCDI climate indices.

2.3 | Methods

2.3.1 | Climate indices

Table 2 lists the names and definitions of the rainfall-related climate indices computed in this study. The definitions of the climate indices have been adopted from the ETCCDI team (Klein Tank *et al.*, 2009). The indices were calculated using the package developed by Schulzweida and Quast (2015), which is part of the climate data operator (CDO) suite of routines (Schulzweida *et al.*, 2006). In addition to indices from ETCCDI, we also calculated the number of periods of consecutive dry days (CDD) and consecutive wet days (CWD) that exceed 5 days (CDD5D and CWD5D), which are available in the package created by Schulzweida and Quast (2015). Moron *et al.* (2009) used a 5-day sequence to calculate the onset of the monsoon season using the agronomical definition (Sivakumar, 1988). The climate indices were calculated annually for the period from 1981 to 2005.

2.3.2 | Validation methods

The Taylor diagram (Taylor, 2001) and Kolmogorov-Smirnov (K-S) statistic values are used for the validation

of the models. The Taylor diagram used the ensemble mean of the observed climate indices. This is because this analysis focuses on the pattern similarity between the models and observations. The K-S statistic values were calculated individually using the simulated climate indices from the models and the observed climate indices from the three observational datasets (SA-OBS, APHRODITE, and CHIRPS); then, the final K-S values were calculated from the mean value of these individual K-S scores. This step is intended to avoid biases among the three observational datasets.

We used the Taylor diagram to compare the climatology of the climate indices for the models and observations. The Taylor diagram has been frequently used to evaluate climate models, and it is a suitable analysis tool for this study, as it can summarize how well the modelled and observed patterns match (Taylor, 2001) in terms of the spatial correlation and spatial standard deviation (*SD*). The Taylor diagram shows the spatial correlation on the azimuthal axis, while the *x*-axis and *y*-axis show the normalized *SD*. Both the spatial correlation and *SD* are calculated over space of the climatological condition of the indices on the model and observations. For the normalization, we used the *SD* from the observations. A normalized *SD* equal to one indicates the maximum similarity between the models and observations.

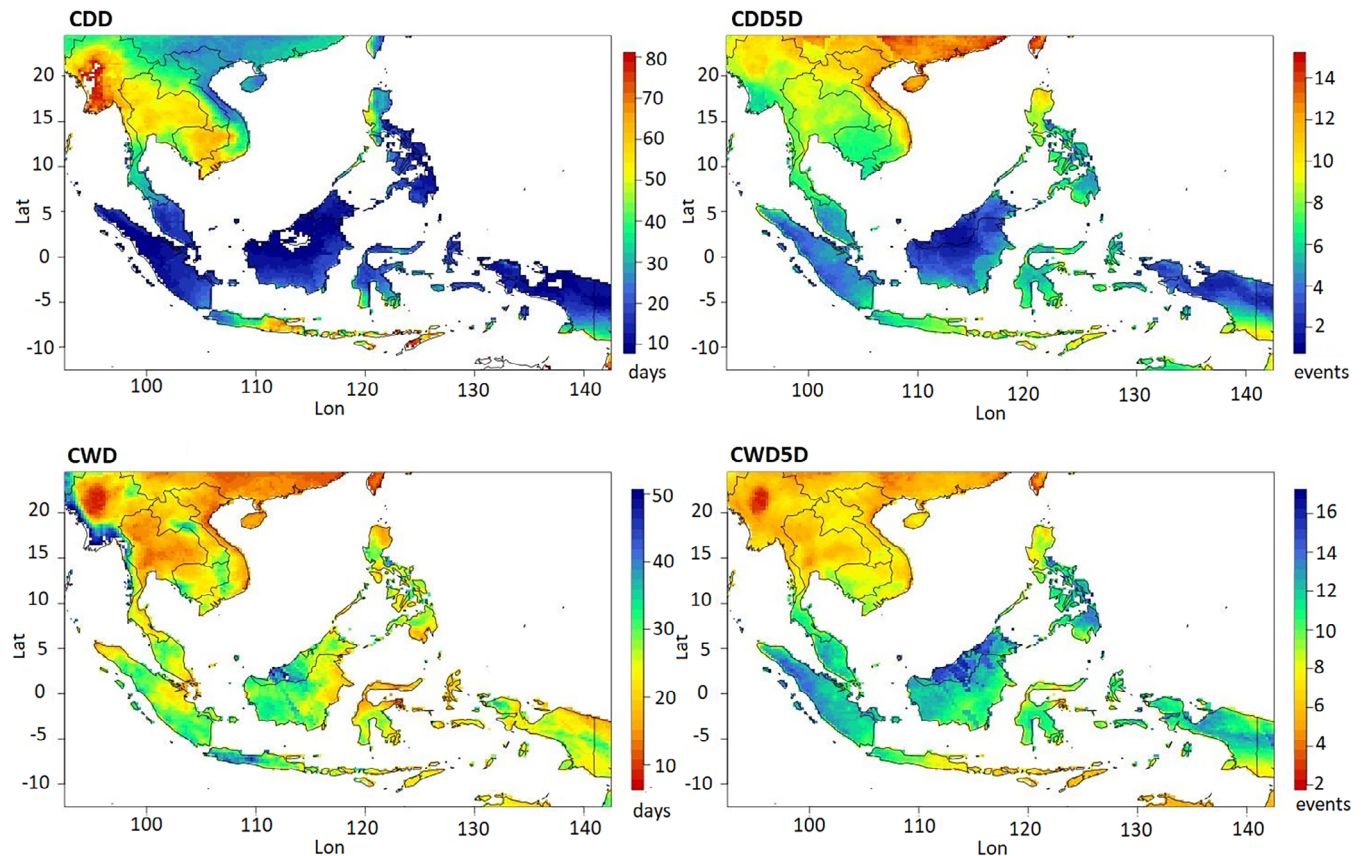


FIGURE 1 Climatological map of the observed annual maximum dry spell length (CDD), annual number of CDDs > 5 days (CDD5D), annual maximum wet spell length (CWD), and annual number of CWDs > 5 days (CWD5D). The indices represent the mean values of indices obtained from observational datasets (SA-OBS, APHRODITE, and CHIRPS) for the period from 1981 to 2005 [Colour figure can be viewed at wileyonlinelibrary.com]

Furthermore, we applied the two-sample K-S statistic to compare the modelled and observed indices. The K-S test statistic shows the distance between two probability distributions, with a low value of the test statistic indicating a high similarity between the two datasets. We applied the K-S test to each grid cell in the study area.

3 | RESULTS

3.1 | Observed climate indices over Southeast Asia

We estimate climatological values to investigate the spatial distributions of the indices from the observations. Figure 1 shows the spatial distribution of the CDD, CDD5D, CWD, and CWD5D values. We find large CDD values (greater than 50 days) over Myanmar, Thailand, Cambodia, and southern Vietnam, where the dry season period occurs from October to May. Meanwhile, for the Indonesia region, large CDD values occur over East Java and Nusa Tenggara in the southern part of the region,

which is the driest province in Indonesia. For CDD5D, we find that the northern part of SEA experiences more than nine of these dry events per year, which is relatively high compared to other regions in SEA. Meanwhile, the spatial distribution of CDD5D over Indonesia shows a similar pattern to the spatial distribution of the CDD index. Rainfall in the southern part of Indonesia has a strong correlation with El Niño, especially during the peak of the dry season from June to August and the onset of the rainy season from September to November (Aldrian and Susanto, 2003; Trouet and Van Oldenborgh, 2013). This causes a series of dry days in the region.

Large climatological CWD values (greater than 30 days) are found over the west coast of Myanmar, Borneo, Sumatra, and Java. Meanwhile, we found a CWD5D value exceeding nine events per year over the region between -5°S and 10°N (equatorial region). The equatorial region is traversed by the ITCZ twice a year (March and September); therefore, there are two monsoon seasons over this region (boreal spring and boreal autumn), leading to high cumulative monthly precipitation throughout the year (Aldrian and Susanto, 2003).

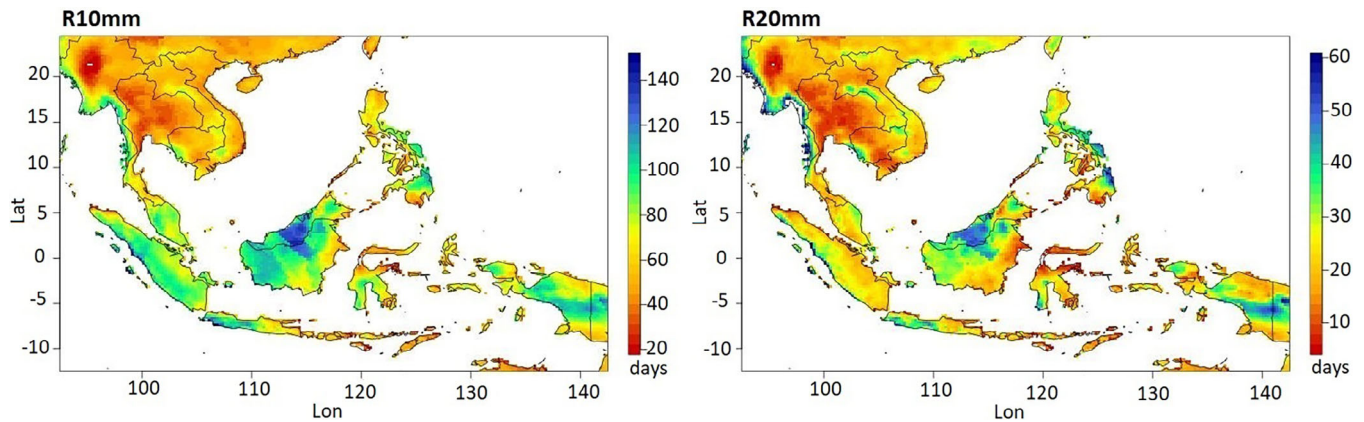


FIGURE 2 Climatological map of the observed annual number of days on which the precipitation is ≥ 10 mm (R10mm) and annual number of days on which the precipitation is ≥ 20 mm (R20mm). The indices represent the mean values of indices obtained from observational datasets (SA-OBS, APHRODITE, and CHIRPS) for the period from 1981 to 2005 [Colour figure can be viewed at wileyonlinelibrary.com]

As shown in Figure 2, heavy (≥ 10 mm) and very heavy (≥ 20 mm) daily precipitation are more frequent (R10mm > 100 days and R20mm > 30 days) over the eastern part of the Philippines and Malaysia. Meanwhile, for the Indonesia region, these events occurred more often over the northern part of Borneo, West and Central Java, and the central part of Papua.

Similar spatial patterns are found for the maximum daily precipitation (Rx1day), maximum 5-day precipitation (Rx5day), and number of 5-day heavy precipitation periods (R5day50mm) (Figure 3). High Rx1day (> 80 mm), Rx5day (> 200 mm), and R5day50mm (> 6 events) values are found over the west coast of Myanmar and the east coast of the northern part of Vietnam, the Malaysian Peninsula, and the Philippines. This is associated with the tropical cyclones that occur in these areas (Nguyen-Thi *et al.*, 2012; Li *et al.*, 2013; Corporal-Lodangco and Leslie, 2017).

Contributions from extreme wet days (R95pTOT) appear to be substantial over the northern part of Vietnam, Thailand, Myanmar, and the Philippines, with values of more than 20% (Figure 4). In addition, simple daily precipitation index (SDII) values from 8 to 12 mm·day⁻¹ are found in most SEA areas. Higher values of the SDII (> 13 mm·day⁻¹) occurred over the west coast of Myanmar and the east coast of the Philippines (Figure 4).

In addition, we find high R95pTOT and SDII values over the east coast of the northern part of Vietnam, Thailand, and the Malaysian Peninsula. The extreme rainfall has a high intensity (Rx1day > 80 mm and Rx5day > 200 mm) over these areas, but the frequencies of heavy and very heavy rainfall events are low (R10mm < 100 days and R20mm < 40 days). These conditions cause a high contribution of extreme wet days to the total rainfall (R95pTOT) and a high SDII. Slightly

different conditions are found for the region over the west coast of Myanmar. Over this area, high values of Rx1day and Rx5day are followed by frequent heavy and very heavy rainfall events. These conditions are responsible for a high total yearly precipitation. As a result, the R95pTOT value is low, whereas the SDII is high for this area. For the eastern part of the Philippines, although R10mm and R20mm are high, we observed a high R95pTOT value. This is due to the very high intensity of extreme rainfall over this area during tropical cyclone events from May to November (Corporal-Lodangco and Leslie, 2017); the proportion of the extreme rainfall of the total precipitation is high even though the total precipitation is also high. Along with a high R95pTOT value, we also observed a high SDII over this area.

Over the Indonesia region, R95pTOT varies from 15 to 25% and the SDII varies from 6 to 14 mm. High R95pTOT values (from 20 to 25%) occur over Nusa Tenggara and also over the southern and northern parts of Papua. Meanwhile, areas like Java, Borneo, Nusa Tenggara, and the centre of Papua have a high SDII value (around 12 mm). The high SDII and the low R95pTOT values over Java, Borneo, and the centre of Papua are related to the high frequency of heavy and very heavy rainfall events. However, for Nusa Tenggara, the high SDII and R95pTOT values are due to a few rainy days over the region, as shown by the CDD, CDD5D, CWD, and CWD5D values.

3.2 | Model performance for climate indices over SEA

The models simulated similar spatial distributions for the majority of the climatological indices. Except for the CWD,

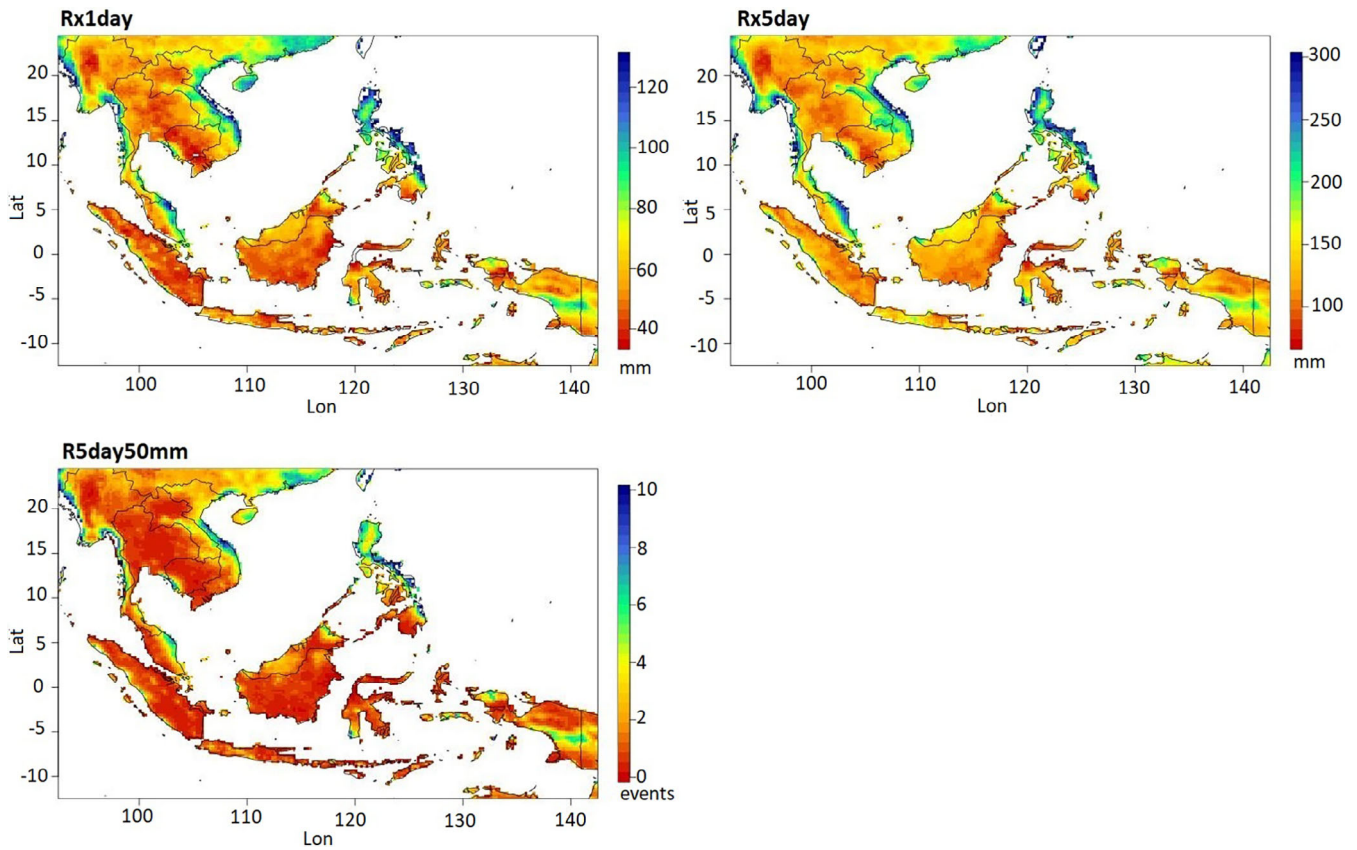


FIGURE 3 Climatological map of the observed annual maximum daily rainfall (Rx1day), annual maximum 5-day rainfall (Rx5day), and annual number of 5-day heavy precipitation periods (R5day50mm). The indices represent the mean values of indices obtained from observational datasets (SA-OBS, APHRODITE, and CHIRPS) for the period from 1981 to 2005 [Colour figure can be viewed at wileyonlinelibrary.com]

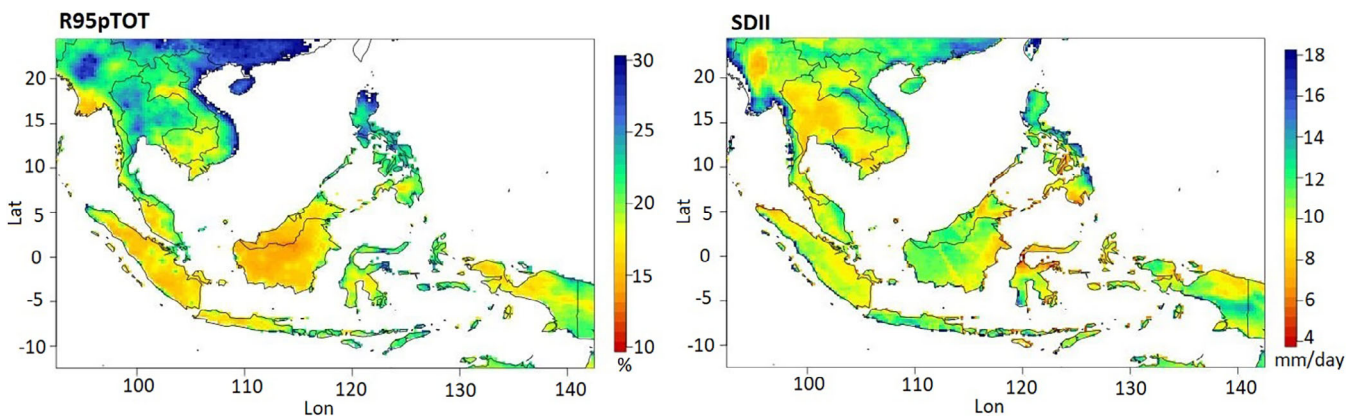


FIGURE 4 Climatological map of the observed annual precipitation percentage due to R95p days (R95pTOT) and annual simple daily intensity index per time period (SDII). The indices represent the mean values of indices obtained from observational datasets (SA-OBS, APHRODITE, and CHIRPS) for the period from 1981 to 2005 [Colour figure can be viewed at wileyonlinelibrary.com]

R20mm, R5D50mm, and SDII values, the spatial correlation is high (>0.50) for most of the models. Based on the normalized *SD* values of the spatial distributions, the models are close to the observations ($0.8 < \text{normalized}$

$SD < 1.2$) in terms of the CDD, CDD5D, CWD5D, and R95pTOT indices.

Figure 5 shows the Taylor diagrams for the simulated CDD, CDD5D, CWD, and CWD5D values. In terms of

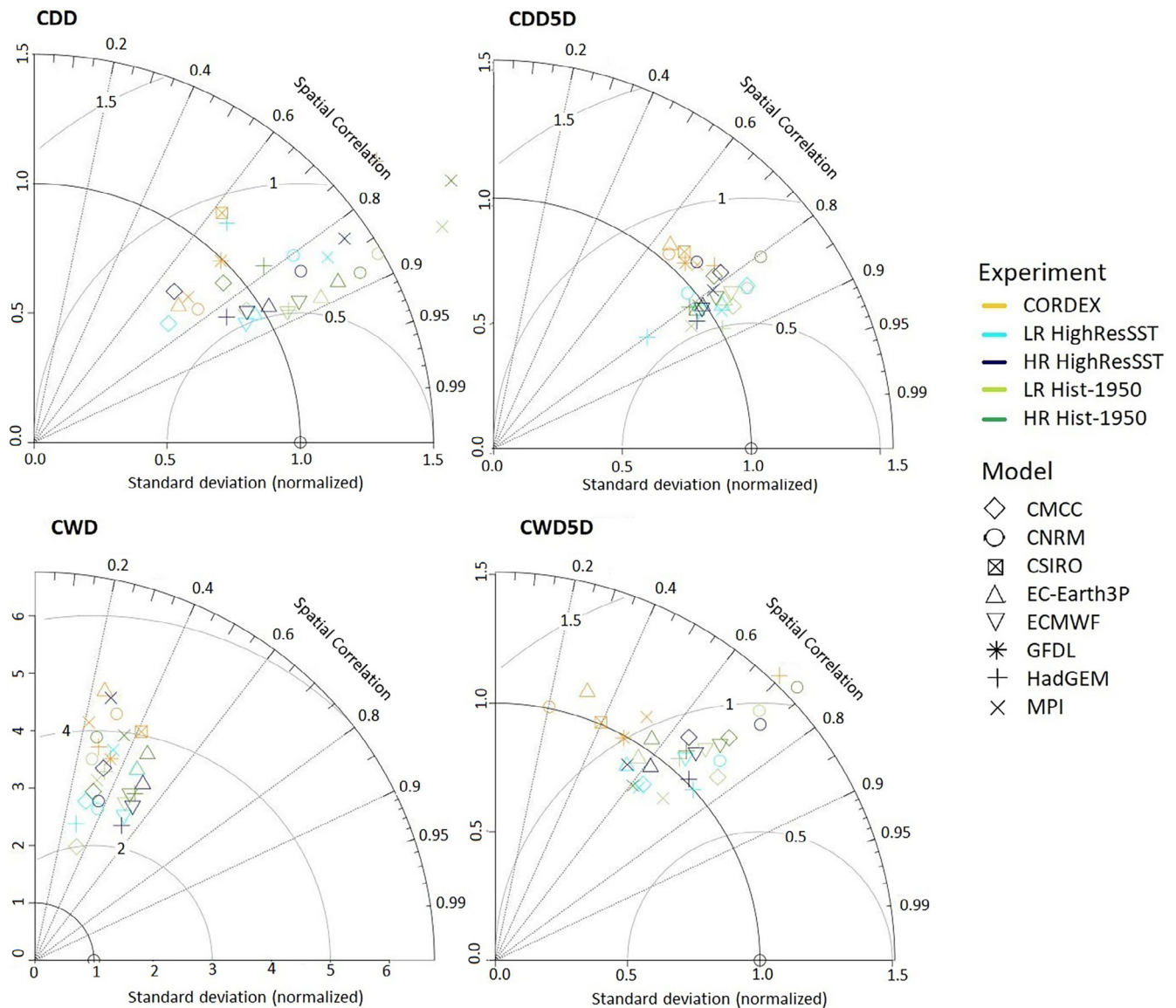


FIGURE 5 Taylor diagrams of the spatial distributions of the simulated annual maximum dry spell length (CDD), annual number of CDDs >5 days (CDD5D), annual maximum wet spell length (CWD), and annual number of CWDs >5 days (CWD5D). The x-axis (y-axis) shows the normalized SD and the azimuthal axis shows the spatial correlation between the models and observations for the indices [Colour figure can be viewed at wileyonlinelibrary.com]

the spatial correlation, HighResMIP (HighResSST and Hist-1950) provides a better simulation than CORDEX. For the CDD and CDD5D values, most of the HighResMIP models show a spatial correlation that is greater than 0.8, whereas all the CORDEX models show a spatial correlation that is less than 0.8. For the CWD values, all model simulations show a low spatial correlation. The majority of the HighResMIP models show a spatial correlation that is greater than 0.35, while only one CORDEX model (CSIRO) reached this value. For CWD5D, a spatial correlation coefficient of greater than 0.5 is seen in all HighResMIP models, whereas only two CORDEX models (HadGEM and MPI) reach this level of agreement with

the observations. We find that Hist-1950 shows a slightly higher spatial correlation than HighResSST. Meanwhile, we find similar spatial correlations for the low-resolution (LR) and high-resolution (HR) HighResMIP models. In general, based on the spatial correlation, the Hist-1950 LR simulations show a stronger resemblance to the observations than the other model experiments.

Based on the normalized SD, CORDEX and HighResMIP have similar performances. The normalized SD values of four CORDEX models for the CDD index range from 0.8 to 1.2, whereas three out of six HighResMIP models for each experiment (HighResSST and Hist-1950 for HR and LR models) are in that range. Similarly, for

CDD5D, all CORDEX models have a normalized *SD* from 0.8 to 1.2, and most of the HighResMIP models have *SD* values within this range as well, except for HadGEM (HighResSST-LR) and CNRM (Hist-1950-HR). For the CWD index, HighResMIP shows a lower *SD* value for the majority of the models, which have normalized *SD* values that are less than 3.5, while all CORDEX models show normalized *SD* values that are greater than 3.5. For the number of wet periods (CWD5D), all the HighResSST-LR models show normalized *SD* values from 0.8 to 1.2, while in CORDEX, HighResSST-LR and Hist-1950-LR, there are five out of six models in this range; four out of six models are in this range for Hist-1950-LR. In the HighResMIP experiments, HighResSST shows a better *SD* value than Hist-1950. Furthermore, for HighResMIP, we find that LR HighResMIP appears to have a slightly better *SD* value than HR HighResMIP. In general, according to the normalized *SD* values of the CDD, CDD5D, CWD, and CWD5D indices, HighResSST-LR provides a better simulation than the other model experiments.

Figure 6 shows the Taylor diagrams for the model simulations of R10mm and R20mm. The HighResMIP models show a higher spatial correlation and lower normalized *SD* than the CORDEX models. In terms of the spatial correlation, for R10mm, only two out of six models in the CORDEX experiment have a spatial correlation that is greater than 0.55, while the majority of the HighResMIP models have spatial correlations exceeding 0.55. The contrast is slightly larger for R20mm. All of the CORDEX models show a spatial correlation that is less than 0.3, whereas the majority of the HighResMIP models show a spatial correlation that is greater than 0.4 and a normalized *SD* that is considerably smaller. Except for the CNRM model (experiment Hist-1950, both HR and LR), all HighResMIP models show *SD* values that are well below those of the CORDEX models, which have normalized *SD* values that are greater than 2 for R10mm and greater than 3 for R20mm. Within the models of HighResMIP, we find similar performances for the HighResSST and Hist-1950 experiments, and the LR and HR experiments. In general, HighResSST-HR shows a higher spatial correlation for R10mm and R20mm than the other experiments. Among the HighResMIP model experiments, HighResSST has an *SD* that is slightly closer to the observations compared to Hist-1950. LR HighResMIP has a slightly smaller normalized *SD* value than HR HighResMIP. In general, for R10mm and R20mm, HighResSST-LR shows a better *SD* than the other experiments.

Figure 7 shows that in general, HighResMIP has a higher spatial correlation and a lower normalized *SD* than CORDEX for Rx1day, Rx5day, and R5day50mm. In terms of the spatial correlation, for Rx1day, while none

of the CORDEX models show a spatial correlation that is greater than 0.5, the majority of the HighResMIP models show spatial correlations that are greater than 0.5. For Rx5day, only one model from CORDEX shows a spatial correlation that is greater than 0.4. For HighResMIP, four models (not MPI and CMCC) show spatial correlations that are greater than 0.4. For R5Day50mm, only one model from CORDEX shows a spatial correlation that is greater than 0.2. This index is also not particularly well simulated by HighResMIP. The spread in the correlation with the observations ranges from close to 0 to 0.6, but the overall similarity to the observations is higher for these models than it is for CORDEX. HighResMIP also outperforms CORDEX in terms of the normalized *SD* for Rx1day, Rx5day, and R5Day50mm. Among the HighResMIP experiments, HighResSST shows a higher spatial correlation than Hist-1950, but the normalized *SD* values for both experiments are comparable. HR HighResMIP shows a higher spatial correlation than LR HighResMIP, except for R5Day50mm. However, LR HighResMIP shows an *SD* value that is closer to the observations compared to HR HighResMIP.

Confirming the findings for the previous indices, we find that HighResMIP has a stronger spatial correlation with the observations than CORDEX for the R95pTOT and SDII values (Figure 8). For R95pTOT, the spatial correlation for all CORDEX models is less than 0.65, while the majority of the HighResMIP models show spatial correlations that are greater than 0.65. For the SDII, only one model from the CORDEX suite (CNRM) shows a spatial correlation that is greater than 0.3, while the majority of HighResMIP models show spatial correlations that are greater than 0.3. Among the HighResMIP model experiments, HighResSST has a slightly higher spatial correlation than Hist-1950. Among the HighResMIP resolutions, LR shows a higher spatial correlation for R95pTOT and a lower spatial correlation for the SDII than HR. In general, for R95pTOT, HighResSST-LR shows a higher spatial correlation than the other experiments. For the SDII, HighResSST-HR shows a higher spatial correlation than the other experiments.

In terms of the *SD*, we find that the CORDEX and HighResMIP models have similar performances for R95pTOT. Except for HadGEM, the CORDEX models show normalized *SD* values from 0.8 to 1.2. For HighResMIP, 66% of the models also show normalized *SD* values from 0.8 to 1.2. In terms of the SDII, HighResMIP has a better *SD* than CORDEX. All CORDEX models show normalized *SD* values that are greater than 2, while the majority of the HighResMIP models show normalized *SD* values that are less than 2, which means that HighResMIP is closer to the observations than CORDEX. We find that HighResSST and Hist-1950 have similar performances for R95pTOT and the SDII based on the *SD*. LR

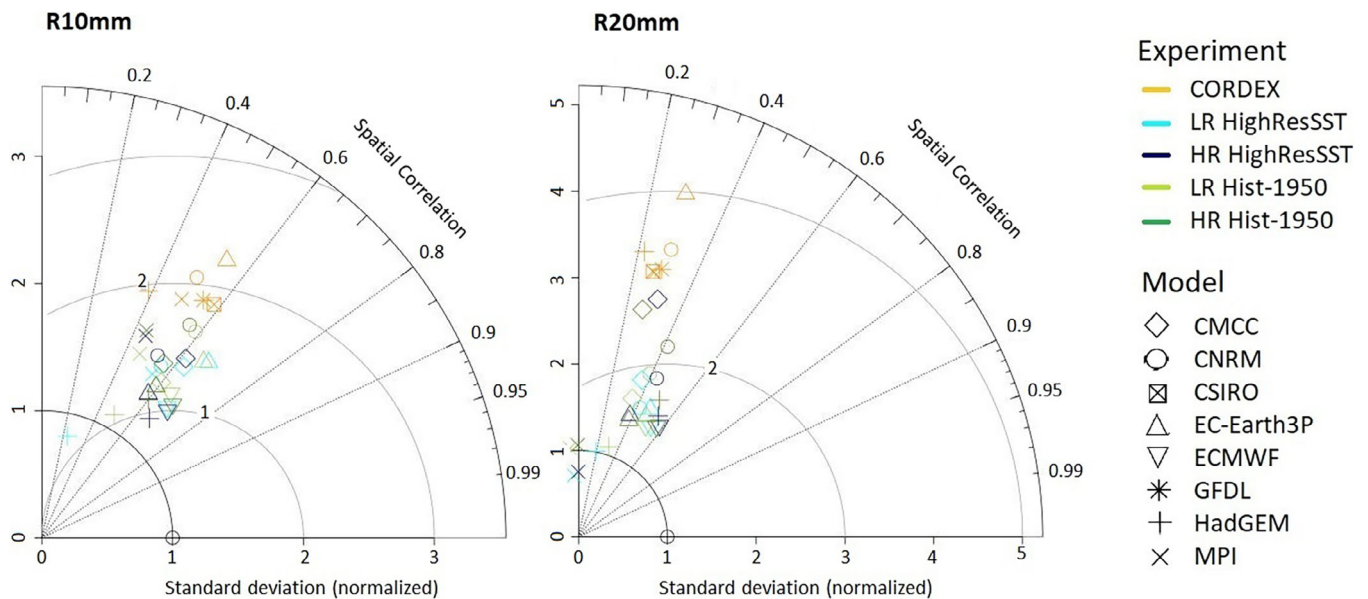


FIGURE 6 Similar to Figure 5, but for the annual number of days on which the precipitation is ≥ 10 mm (R10mm) and annual number of days on which the precipitation is ≥ 20 mm (R20mm) [Colour figure can be viewed at wileyonlinelibrary.com]

HighResMIP is closer to the observations than HR HighResMIP for the SDII, but both resolutions show similar performances for R95pTOT. In general, based on R95pTOT and the SDII, HighResSST-LR shows a better SD than the other experiments.

3.3 | Kolmogorov–Smirnov test of the simulated climate indices over SEA

The K-S test is a method for investigating if two probability distributions can be regarded as indistinguishable from each other or if an underlying probability distribution differs from a hypothesised distribution. In this study, the K-S statistic values are calculated from the yearly time series of the climate indices for each grid box over land. The K-S distributions are plotted using boxplots in Figures S1–S11, Supporting Information. Figure 9 shows the median values of the spatial distribution of the K-S statistics for each climate index for each model. Based on the K-S analysis, the HighResMIP experiments (HighResSST and Hist-1950) show consistently lower values than CORDEX, which shows that the simulated climate indices from HighResMIP have distributions that are closer to the observations compared to the CORDEX simulation. This shows that the HighResSST and Hist-1950 experiments are closer to the distribution of the observed climate indices compared to the CORDEX models.

For the CDD and CDD5D indices, the majority of the CORDEX models show K-S values above 0.5. For

HighResMIP, except for CMCC with HighResSST, all of the models show K-S values below 0.5 (Figures 9, S1, and S2). On the contrary, most of the models for both CORDEX and HighResMIP show K-S values that are greater than 0.75 for the CWD index. Except for HadGEM, all of the CORDEX models show K-S values greater than 0.85; they show higher K-S values than HighResMIP. There is one model for HighResSST LR and HR that has a K-S value of greater than 0.85. For the Hist-1950 experiment, there are three LR models and two HR models that have K-S values that are greater than 0.85 (Figures 9 and S3). In addition, for CWD5D, most of the median K-S values for CORDEX are greater than 0.4. The following HighResMIP models have a median K-S value of greater than 0.4: one model for HighResSST LR, two models for HighResSST HR, four models for Hist-1950 LR, and three models for Hist-1950 HR (Figures 9 and S4). For the CDD, CDD5D, CWD, and CWD5D indices, we find similar performances for different HighResMIP experiments and for the LR and HR HighResMIP experiments.

In terms of R10mm and R20mm, all CORDEX models show median K-S values that are greater than or equal to 0.7. For HighResMIP, only one model (HadGEM in the HighResSST LR experiment) shows a similar disagreement with the observations on R10mm (Figures 9 and S5). For R20mm, there are two models (HadGEM and MPI) for HighResSST LR that have median K-S values of greater than or equal to 0.7 and one model (MPI) that reaches this K-S value for the other experiments (Figures 9 and S6). Based on R10mm and R20mm, HighResSST has a slightly better performance than

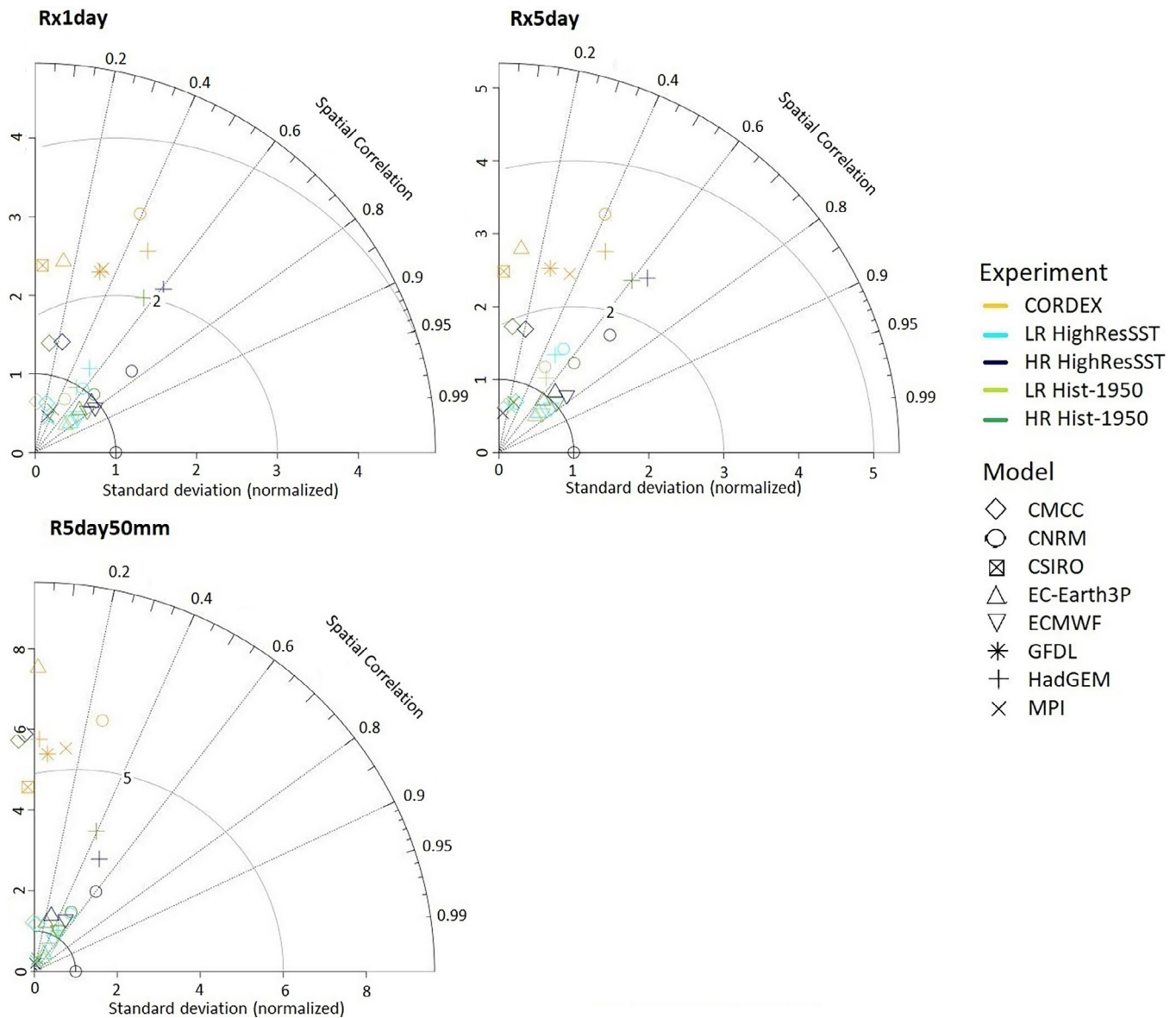


FIGURE 7 Similar to Figure 5, but for the annual maximum daily rainfall (Rx1day), annual maximum 5-day rainfall (Rx5day), and annual number of 5-day heavy precipitation periods (R5day50mm) [Colour figure can be viewed at wileyonlinelibrary.com]

Hist-1950. We find similar performances for LR and HR HighResMIP.

In addition, for Rx1day, Rx5day, and R5day50mm, compared to CORDEX, whose models show K-S values that are greater than 0.5 (Rx1day and R5day50mm) and greater than or equal to 0.75 (Rx5day), the HighResSST models show a stronger similarity with the observations. In terms of Rx1day, three Hist-1950 models (CNRM, HadGEM, and ECMWF) and two models (CNRM and ECMWF) from other HighResMIP experiments show median K-S values that are less than 0.5 (Figures 9 and S7). For Rx5day, there is only one model (CMCC) from the HR HighResSST and Hist-1950 experiments that shows a median K-S value of greater than or equal to

0.75 (Figures 9 and S8). Meanwhile, for R5day50mm, there is only one LR model (CMCC) and two models (HadGEM and CMCC) from the HighResSST and Hist-1950 experiments that have median K-S values of greater than 0.5 (Figures 9 and S9). Based on the K-S analysis of the Rx1day, Rx5day, and R5day50mm indices, we find that all HighResMIP experiments perform about equally well. LR HighResMIP shows slightly lower K-S values than HR HighResMIP, especially for R5day50mm.

In contrast to the results of the analysis of the previous indices, the performance of HighResMIP does not exceed the performance of CORDEX for R95pTOT and the SDII according to the K-S values. In terms of R95pTOT, all CORDEX models show median K-S values

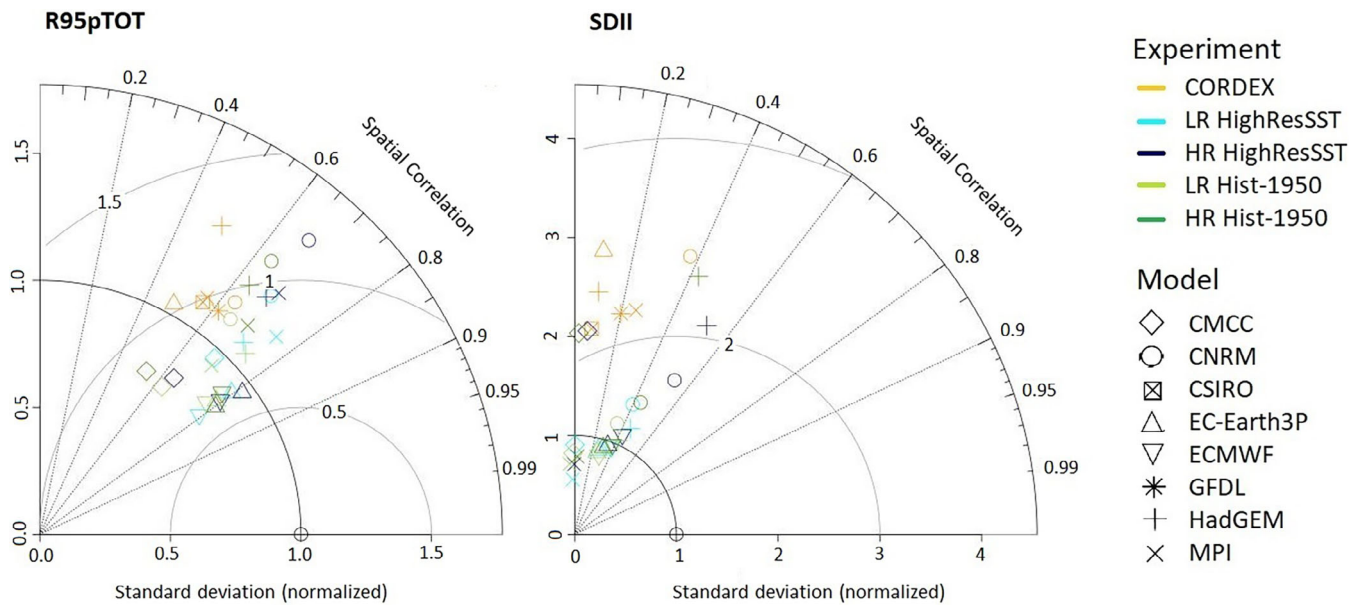


FIGURE 8 Similar to Figure 5, but for the annual precipitation percentage due to R95p days (R95pTOT) and annual simple daily intensity index per time period (SDII) [Colour figure can be viewed at wileyonlinelibrary.com]

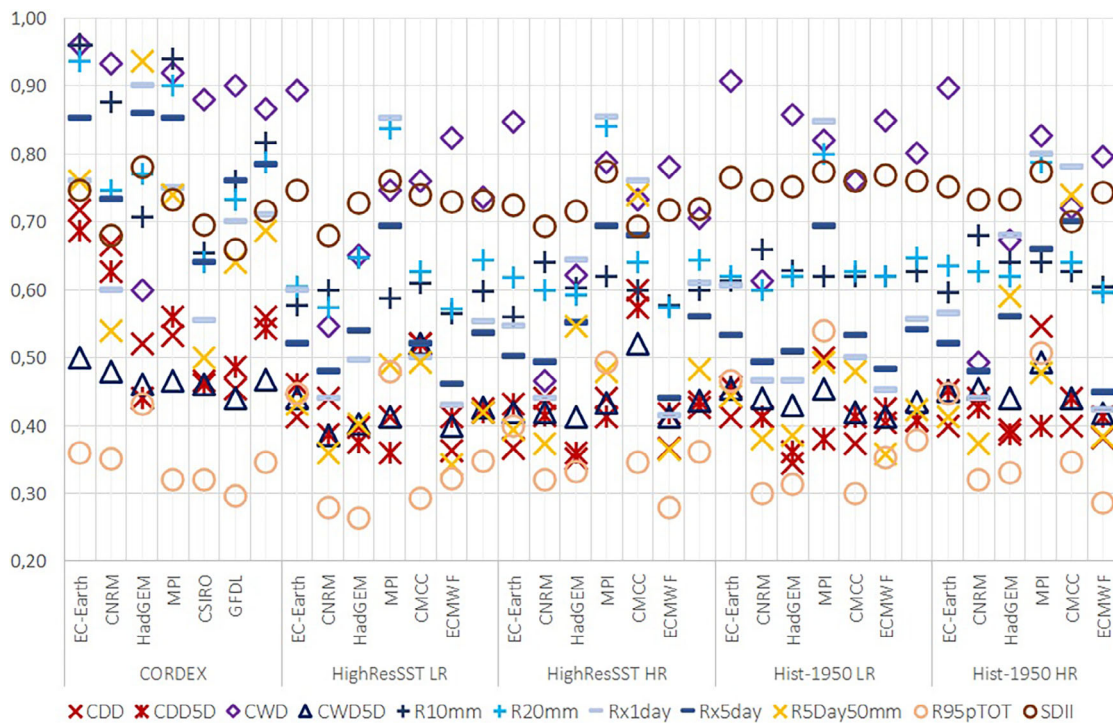


FIGURE 9 Median K-S statistic values of the simulated climate indices. The K-S statistic is calculated for each grid point that is located over land. The median value is calculated from the spatial distribution of the K-S statistic [Colour figure can be viewed at wileyonlinelibrary.com]

of less than 0.45 (Figures 9 and S10). Meanwhile, for HighResMIP, two models (EC-Earth and MPI) show median K-S values that are greater than or equal to 0.45. In addition, similar performances in terms of the SDII

are found for CORDEX and HighResMIP (Figures 9 and S11). Based on R95pTOT and the SDII, HighResSST has a slightly better performance than Hist-1950. We find similar performances for LR and HR HighResMIP.

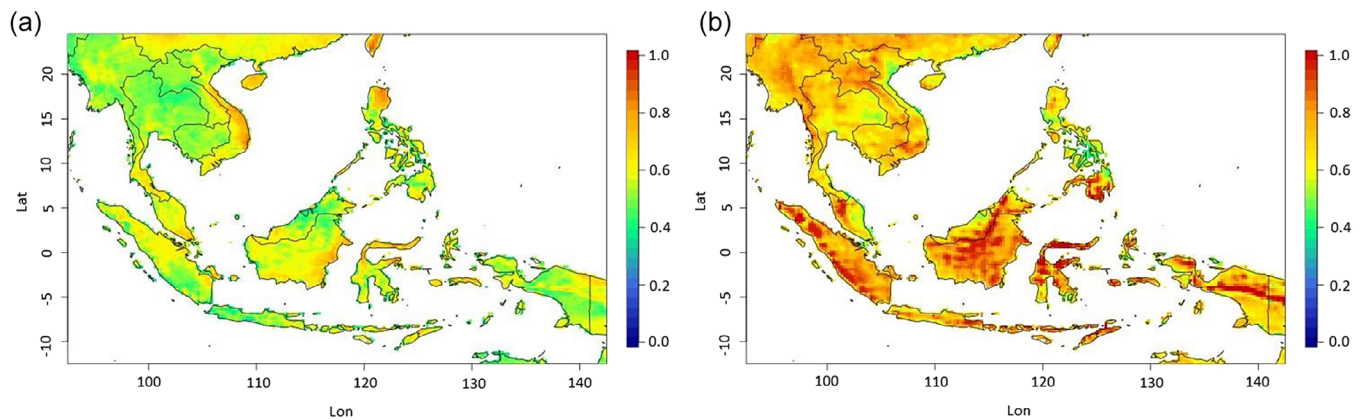


FIGURE 10 Kolmogorov–Smirnov index map of CORDEX simulations of (a) climate indices that are related to climatological conditions (CDD, CDD5D, CWD, CWD5D, and R95pTOT) and (b) climate indices that are directly related to the rainfall intensity (R10mm, R20mm, Rx1day, Rx5day, R5day50mm, and SDII) [Colour figure can be viewed at wileyonlinelibrary.com]

4 | DISCUSSION

We used three gridded precipitation observational datasets in this study to account for the low dispersion of gauge data in SEA. SA-OBS and APHRODITE were developed from rain gauges. SA-OBS, which was developed specifically for the SEA region, has a higher station density compared to APHRODITE, which was developed for the Asia region. However, due to the restriction in the interpolation method, the spatial coverage of SA-OBS is lower than that of APHRODITE over SEA. The CHIRPS dataset is based on a satellite rainfall retrieval algorithm that combines climatology data, satellite precipitation estimates, and an in situ rain gauge. This means that CHIRPS provides more complete coverage over SEA compared to SA-OBS and APHRODITE. However, the amount of rain gauge data used for calibration in CHIRPS is considerably lower than the amount of rain gauge data used in SA-OBS and APHRODITE. For the extremes, the precipitation value of a grid square should be seen as an area average for that grid square. This means that extremes will be “smeared” out more in datasets with a coarser resolution (Van den Besselaar *et al.*, 2017).

We determine the similarity of the three gridded precipitation observational datasets using K-S values for the eleven rainfall-related climate indices. We find that the similarity between APHRODITE and CHIRPS is the lowest; they have the highest K-S index in this comparison of observational datasets. SA-OBS and APHRODITE have the highest similarity (Figure S12). This confirms the results of a previous study by Van den Besselaar *et al.* (2017), who found that the similarities between gauge-based datasets are higher than the similarities between gauge-based datasets and satellite-based datasets.

Based on the K-S indices for the observational datasets, we find that the three observational datasets have

a low similarity in the area over south China and the southwest coast of Myanmar (Figure S13). The area of low similarity is spread over more of SEA for APHRODITE and CHIRPS. For SA-OBS and APHRODITE, some low-similarity zones are also found in some areas of Indonesia, such as the centre of Sumatra. For SA-OBS and CHIRPS, zones of low similarity were also found in some areas in Vietnam, Cambodia, and Indonesia (Papua Island). The low similarity between the observational datasets for some areas like Papua and Myanmar is caused by the low density of the data available over the area that are used to develop the observation datasets. However, the areas where the observational datasets diverge most are not the areas where the spatial patterns of the model precipitation fields differ most from the mean in the observational datasets. Nevertheless, this shows the need for the further development of the observational datasets for this region. In addition, the use of multiple observational datasets of the region can reduce the uncertainty.

Eleven different rainfall-related climate indices were used to investigate the performance of different generations of climate models. Among the 11 indices, the CORDEX and HighResMIP models are better at simulating rainfall indices that show climatological characteristics (climatic rainfall indices: CDD, CDD5D, CWD, CWD5D, and R95pTOT) and slightly worse at simulating rainfall indices that are more directly related to the rainfall intensity (R10mm, R20mm, Rx1day, Rx5day, and R5day50mm).

For the climatic rainfall indices, both the CORDEX and HighResMIP models are better at simulating R95pTOT and worse at simulating CWD compared to the other indices. In general, the models produce worse simulations over the antimonsoon region (5°S–2°N and 120°–135°E). This poor performance is worse in the CORDEX simulation because the low performance of the

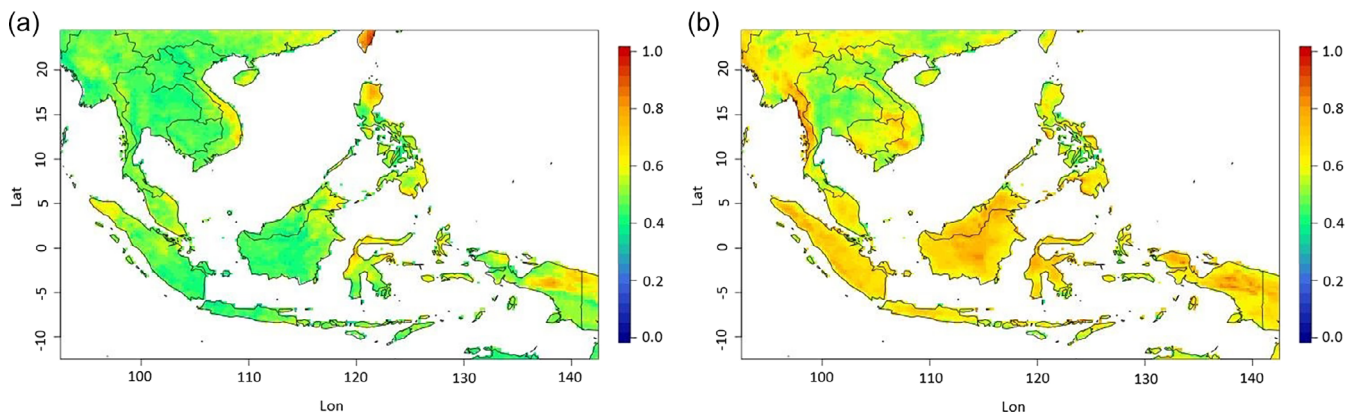


FIGURE 11 Kolmogorov–Smirnov index map of Hist-1950 HR simulations of (a) climate indices that are related to climatological conditions (CDD, CDD5D, CWD, CWD5D, and R95pTOT) and (b) climate indices that are directly related to the rainfall intensity (R10mm, R20mm, Rx1day, Rx5day, R5day50mm, and SDII) [Colour figure can be viewed at [wileyonlinelibrary.com](https://onlinelibrary.wiley.com/doi/10.1002/joc.7938)]

simulation is spread out over the equatorial region (5°S–10°N). The advantage of the prescribed SST in HighResSST is shown; it results in a better simulation than CORDEX. The comparable performances of Hist-1950 and HighResSST show the skill of the ocean model in Hist-1950. In a previous study, Hist-1950 also demonstrated a better seasonal southward migration of the rain band from the Asian summer monsoon to the Australian summer monsoon and better monsoon season rainfall simulations over SEA compared to CORDEX (Hariadi *et al.*, 2021). We assume that one of the reasons for this is that HighResMIP has the advantage of a global-scale run, while CORDEX has only a regional-scale run. Furthermore, Kamruzzaman *et al.* (2021) found that CMIP6 provides a better simulation of the Indian summer monsoon than CMIP5. CMIP6 also simulated better seasonal characteristics over the western North Pacific and East Asia region (Chen *et al.*, 2021).

In addition, both model experiments also show a poorer simulation of Vietnam and the northern Philippines. This poor performance is worse in CORDEX than in HighResMIP. The area is affected by tropical cyclones. A previous study by Park *et al.* (2021) found that CMIP6 models are better than CMIP5 models at simulating the pattern correlations and thermodynamic conditions of the tropical cyclones that affect the South Korean region.

For rainfall indices that are directly related to the intensity characteristic, both climate model experiments (CORDEX and HighResMIP) are generally worse at simulating the extreme precipitation over the mountainous region (Figures 10, 11, S14, and S15). This highlights the need for improvement in the representation of the physical processes of orographic regions in climate models (Raïsaänen, 2007; Elvidge *et al.*, 2019). CORDEX performs worse than HighResMIP. Demory *et al.* (2020a)

found a similar result when they studied heavy precipitation in Europe. They found that the heavy rainfall that is simulated by HighResMIP is closer to the observations than the heavy rainfall that is simulated by EURO-CORDEX.

Even though HighResMIP shows better climatic rainfall indices than CORDEX, and the previous study by Hariadi *et al.* (2021) also shows a better simulation of monsoon characteristics, finding that Hist-1950 has better and comparable performances compared to CORDEX for intensity-related precipitation indices is unexpected. This is because Hist-1950 was the higher resolution version of the CMIP6 General Circulation Models (GCM) that was originally developed at a coarser resolution and has little additional tuning. On the other hand, CORDEX is the downscaling result of CMIP5, which was developed at a higher resolution and potentially tuned at each resolution (Demory *et al.*, 2020b). However, the tuning that was performed during the downscaling process of the CORDEX-SEA version that was used in this study caused more uncertainty in the results. Juneng *et al.* (2016) found a large positive precipitation bias due to the convection scheme that was used in the RegCM4 configuration. This explains the large precipitation biases in the CORDEX-SEA simulation that were found in previous studies (Amsal *et al.*, 2019; Hariadi *et al.*, 2021; Nguyen-Thi *et al.*, 2021). Furthermore, Nguyen *et al.* (2022) found more intensity of daily precipitation in CORDEX-SEA than their forcing GCM. They suggest that the RCM setup (e.g., parameterization scheme) has a more significant role in the model's ability to simulate precipitation compared to its forcing GCM. Tangang *et al.* (2020) discussed the need to improve the RCM simulation in the future for the CORDEX-SEA model and the need to use the latest CMIP models, which helps to reduce the biases. Bias correction on climate model results dataset over this

region is also recommended for the further use of the dataset (Ratri *et al.*, 2019; 2021; Trinh-Tuan *et al.*, 2019; Tangang *et al.*, 2020).

Tangang *et al.* (2018) investigated anomalies in four indices of extreme precipitation: the annual total precipitation on wet days (PRCPTOT), the CDD index, the annual number of days on which the daily precipitation exceeded 50 mm (R50mm), and RX1day. They found that CORDEX-SEA simulations reasonably captured the characteristics of the extreme rainfall anomalies over SEA during the period from 1986 to 2005. Furthermore, in this study, we found that the HighResMIP simulation of extreme precipitation over the region was better than the CORDEX simulation.

5 | CONCLUSION

This study explored how well the HighResMIP and CORDEX models simulated extreme rainfall-related climate indices over the SEA region for the period from 1981 to 2005. There is also a further investigation into whether the latest HighResMIP model experiment is better than the downscaled results of the previous model experiment, CMIP5. These indices cover both the high/wet end of the spectrum and the dry spells. The number of heavy rainfall days (R10mm), number of very heavy rainfall days (R20mm), maximum daily rainfall (Rx1day), maximum 5-day rainfall (Rx5day), number of 5-day heavy precipitation periods (R5day50mm), and simple daily intensity index (SDII) are directly related to the rainfall intensity, and together with the precipitation percentage due to R95p days (R95pTOT), they represent extreme wet conditions. The other four indices (maximum dry spell length [CDD], number of CDDs >5 days [CDD5D], maximum wet spell length [CWD], and number of CWDs >5 days [CWD5D]) are related to the rainy/dry spells. We find that areas affected by tropical cyclones show high extreme rainfall indices (Rx1day and Rx5day) compared to other areas. As a result, R95pTOT and the SDII are also high for most of these areas, except for the west coast of Myanmar, which has a relatively low R95pTOT value due to high R10mm and R20mm values. For the majority of the Indonesia region, high values of the simple SDII are found, and the contribution of rainfall on extreme wet days to the total precipitation (R95pTOT) is low, except for Nusa Tenggara, which is the driest area in the region. This is due to the high R10mm and R20mm values found for the majority of the Indonesia region; they result in a high total yearly precipitation.

The similarity between the CORDEX and HighResMIP models and the observations is higher for the CDD, CDD5D, CWD5D, and R95pTOT indices than it is for the

R10mm, R20mm, Rx1day, Rx5day, Rx50mm5day, and SDII values. We can conclude that the models are worse at simulating the rainfall climate indices that are directly related to the rainfall intensity, and they are better at simulating other indices that are not directly related to the rainfall intensity. However, the models provide a good representation of the climatic rainfall conditions. The models can simulate the rainfall pattern and distribution well but still show bias when it comes to the rainfall intensity. This bias is shown in all model experiments but is higher in CORDEX than in HighResMIP.

Overall, HighResMIP is consistently better than CORDEX at simulating the rainfall-related climate indices. Within the HighResMIP experiment, we do not find a significant difference in performance between coupled (Hist-1950) and non-coupled (HighResSST) models when they are used to simulate the indices. This shows the high accuracy of the ocean model used in the coupled models. Moreover, we also find no difference between using HR HighResMIP and using LR HighResMIP.

AUTHOR CONTRIBUTIONS

Gerard van der Schrier: Conceptualization; resources; supervision; writing – review and editing. **Gert-Jan Steeneveld:** Conceptualization; resources; supervision; writing – review and editing. **Dian Nur Ratri:** Writing – review and editing. **Ardhasena Sopaheluwakan:** Conceptualization; resources; supervision. **Albert Klein Tank:** Conceptualization; supervision. **Edvin Aldrian:** Supervision. **Dodo Gunawan:** Resources. **Marie Pierre Moine:** Resources. **Alessio Bellucci:** Resources. **Retish Senan:** Resources. **E Tourigny:** Resources. **Dian Putrasahan:** Resources. **Ajie Linarko:** Resources.

ACKNOWLEDGEMENTS

The first author received funding from the Indonesia Endowment Fund for Education (LPDP) (S-353/LPDP.3/2019) for his PhD program. The second author acknowledges the support of the Royal Netherlands Embassy in Jakarta, Indonesia, through a Joint Cooperation Programme between Dutch and Indonesian research institutes. We are grateful for the SA-OBS dataset and the data providers who are part of the SACA&D project (<http://sacad.database.bmkg.go.id/>). The HighResMIP simulations have been made available through the PRIMAVERA project. This project received funding from the European Union's Horizon 2020 Research and Innovation Programme under grant agreement No. 641727, which also provided support to authors Marie-Pierre Moine, Alessio Bellucci, Retish Senan, Etienne Tourigny, and Dian Putrasahan. Access to PRIMAVERA data at JASMIN is part of the IS-ENES3 project, which has received funding from the European Union's Horizon

2020 Research and Innovation Programme under grant agreement No. 824084. The Etienne Tourigny also received funding from the Research and Innovation Programme under the Marie Skłodowska-Curie grant agreement No. 748750 (SPFireSD project).

ORCID

Mugni Hadi Hariadi  <https://orcid.org/0000-0003-3617-1277>

Ardhasena Sopaheluwakan  <https://orcid.org/0000-0002-4532-854X>

REFERENCES

- Aldrian, E. and Susanto, D. (2003) Identification of three dominant rainfall regions within Indonesia and their relationship to sea surface temperature. *International Journal of Climatology*, 23(12), 1435–1454. <https://doi.org/10.1002/joc.950>.
- Amnuaylojaroen, T. (2021) Projection of the precipitation extremes in Thailand under climate change scenario RCP8.5. *Frontiers in Environmental Science*, 9, 657810. <https://doi.org/10.3389/fenvs.2021.657810>.
- Amnuaylojaroen, T. and Chanvichit, P. (2019) Projection of near-future climate change and agricultural drought in mainland Southeast Asia under RCP8.5. *Climatic Change*, 155(2), 175–193. <https://doi.org/10.1007/s10584-019-02442-5>.
- Amsal, F., Harsa, H., Sopaheluwakan, A., Linarka, U., Pradana, R. and Satyaningsih, R. (2019) Bias correction of daily precipitation from downscaled CMIP5 climate projections over the Indonesian region. *IOP Conference Series: Earth and Environmental Science*, 303, 012046.
- Chang, C.-P., Wang, Z., McBride, J. and Liu, C.-H. (2005) Annual cycle of Southeast Asia—maritime continent rainfall and the asymmetric monsoon transition. *Journal of Climate*, 18(2), 287–301. <https://doi.org/10.1175/JCLI-3257.1>.
- Chen, C.-A., Hsu, H.-H. and Liang, H.-C. (2021) Evaluation and comparison of CMIP6 and CMIP5 model performance in simulating the seasonal extreme precipitation in the western North Pacific and East Asia. *Weather and Climate Extremes*, 31, 100303.
- Cherchi, A., Fogli, P.G., Lovato, T., Peano, D., Iovino, D., Gualdi, S., Masina, S., Scoccimarro, E., Materia, S., Bellucci, A., and Navarra, A. (2019) Global mean climate and main patterns of variability in the CMCC-CM2 coupled model. *Journal of Advances in Modeling Earth Systems*, 11(1), 185–209. <https://doi.org/10.1029/2018MS001369>.
- Corporal-Lodangco, I.L. and Leslie, L.M. (2017) Climatology of Philippine tropical cyclone activity: 1945–2011. *International Journal of Climatology*, 37(9), 3525–3539.
- Davies, R. (2021) Indonesia—floods worsen in greater Jakarta region, 5 people reported dead, over 30,000 displaced. *floodlist*. Available at: <https://floodlist.com/asia/indonesia-greater-jakarta-floods-update-february-2021>.
- Demory, M.-E., Berthou, S., Fernández, J., Sørland, S.L., Brogli, R., Roberts, M.J., Beyerle, U., Seddon, J., Haarsma, R., Schär, C., Buonomo, E., Christensen, O.B., Ciarlò, J.M., Fealy, R., Nikulin, G., Peano, D., Putrasahan, D., Roberts, C.D., Senan, R., Steger, C., Teichmann, C. and Vautard, R. (2020a) European daily precipitation according to EURO-CORDEX regional climate models (RCMs) and high-resolution global climate models (GCMs) from the High-Resolution Model Inter-comparison Project (HighResMIP). *Geoscientific Model Development*, 13(11), 5485–5506. <https://doi.org/10.5194/gmd-13-5485-2020>.
- Demory, M.-E., Berthou, S., Sørland, S.L., Roberts, M.J., Beyerle, U., Seddon, J., Haarsma, R., Schär, C., Christensen, O.B., Fealy, R., Fernandez, J., Nikulin, G., Peano, D., Putrasahan, D., Roberts, C. D., Steger, C., Teichmann, C., and Vautard, R. (2020b) Can high-resolution GCMs reach the level of information provided by 12–50km CORDEX RCMs in terms of daily precipitation distribution? *Geoscientific Model Development*, 2020, 1–33. <https://doi.org/10.5194/gmd-2019-370>.
- Elvidge, A.D., Sandu, I., Wedi, N., Vosper, S.B., Zadra, A., Boussetta, S., Bouyssel, F., van Niekerk, A., Tolstykh, M.A. and Ujiie, M. (2019) Uncertainty in the representation of orography in weather and climate models and implications for parameterized drag. *Journal of Advances in Modeling Earth Systems*, 11(8), 2567–2585. <https://doi.org/10.1029/2019MS001661>.
- ESCAP, UN. (2020) *The disaster riskscape across South-east Asia: key takeaways for stakeholders*. Available at: <https://hdl.handle.net/20.500.12870/3952>.
- FAO. (2021) *The Impact of Disasters and Crises on Agriculture and Food Security: 2021*. Rome: FAO.
- Ferrett, S., Yang, G.-Y., Woolnough, S.J., Methven, J., Hodges, K. and Holloway, C.E. (2020) Linking extreme precipitation in Southeast Asia to equatorial waves. *Quarterly Journal of the Royal Meteorological Society*, 146(727), 665–684. <https://doi.org/10.1002/qj.3699>.
- Funk, C., Peterson, P., Landsfeld, M., Pedreros, D., Verdin, J., Shukla, S., Husak, G., Rowland, J., Harrison, L., Hoell, A. and Michaelsen, J. (2015) The climate hazards infrared precipitation with stations—a new environmental record for monitoring extremes. *Scientific Data*, 2, 150066. <https://doi.org/10.1038/sdata.2015.66>.
- Giorgi, F., Coppola, E., Solmon, F., Mariotti, L., Sylla, M., Bi, X., Elguindi, N., Diro, G., Nair, V., Giuliani, G., Turuncoglu, U.U., Cozzini, S., Güttler, I., O'Brien, T.A., Tawfik, A.B., Shalaby, A., Zakey, A.S., Steiner, A.L., Stordal, F., Sloan, L.C. and Brankovic, C. (2012) RegCM4: model description and preliminary tests over multiple CORDEX domains. *Climate Research*, 52, 7–29. <https://doi.org/10.3354/cr01018>.
- Haarsma, R., Acosta, M., Bakhshi, R., Bretonnière, P.-A.B., Caron, L.-P., Castrillo, M., Corti, S., Davini, P., Exarchou, E., Fabiano, F., Fladrich, U., Fuentes Franco, R., Garca-Serrano, J., von Hardenberg, J., Koenigk, T., Levine, X., Meccia, V., van Noije, T., van den Oord, G., Palmeiro, F.M., Rodrigo, M., Ruprich-Robert, Y., Le Sager, P., Tourigny, E., Wang, S., van Weele, M. and Wyser, K. (2020) HighResMIP versions of EC-Earth: EC-Earth3P and EC-Earth3P-HR. Description, model performance, data handling and validation. *Geoscientific Model Development*, 2020, 1–37. <https://doi.org/10.5194/gmd-2019-350>.
- Haarsma, R.J., Roberts, M.J., Vidale, P.L., Senior, C.A., Bellucci, A., Bao, Q., Chang, P., Corti, S., Fućkar, N.S., Guemas, V., von Hardenberg, J., Hazeleger, W., Kodama, C., Koenigk, T., Leung, L.R., Lu, J., Luo, J.J., Mao, J., Mizielinski, M.S., Mizuta, R., Nobre, P., Satoh, M., Scoccimarro, E., Semmler, T.,

- Small, J. and von Storch, J.S. (2016) High Resolution Model Intercomparison Project (HighResMIP v1. 0) for CMIP6. *Geoscientific Model Development*, 9(11), 4185–4208. <https://doi.org/10.5194/gmd-9-4185-2016>.
- Hamada, J.-I., Yamanaka, M., Matsumoto, J., Fukao, S., Winarso, P. A. and Sribimawati, T. (2002) Spatial and temporal variations of the rainy season over Indonesia and their link to ENSO. *Journal of the Meteorological Society of Japan. Ser. II*, 80(2), 285–310. <https://doi.org/10.2151/jmsj.80.285>.
- Hariadi, M.H., van der Schrier, G., Steeneveld, G.J., Sopaheluwakan, A., Klein Tank, A.M.G., Roberts, M.J., Moine, M.P., Bellucci, A., Senan, R., Tourigny, E. and Putrasahan, D. (2021) Evaluation of onset, cessation and seasonal precipitation of the Southeast Asia rainy season in CMIP5 regional climate models and HighResMIP global climate models. *International Journal of Climatology*, 42, 3007–3024. <https://doi.org/10.1002/joc.7404>.
- IFRC. (2019) *Indonesia: drought information bulletin*. Available at: <https://reliefweb.int/report/indonesia/indonesia-drought-information-bulletin>.
- IPCC. (2021) In: Masson-Delmotte, V., Zhai, P., Pirani, A., Connors, S.L., Péan, C., Berger, S., Caud, N., Chen, Y., Goldfarb, L., Gomis, M.I., Huang, M., Leitzell, K., Lonnoy, E., Matthews, J.B.R., Maycock, T.K., Waterfield, T., Yelekçi, O., Yu, R. and Zhou, B. (Eds.) *Climate Change 2021: The Physical Science Basis. Contribution of Working Group I to the Sixth Assessment Report of the Intergovernmental Panel on Climate Change*. Geneva: IPCC. <https://doi.org/10.1017/9781009157896>.
- Juneng, L., Tangang, F., Chung, J.X., Ngai, S.T., Tay, T.W., Narisma, G., Cruz, F., Phan-Van, T., Ngo-Duc, T., Santisirisomboon, J., Singhruck, P., Gunawan, D. and Aldrian, E. (2016) Sensitivity of Southeast Asia rainfall simulations to cumulus and air-sea flux parameterizations in RegCM4. *Climate Research*, 69(1), 59–77. <https://doi.org/10.3354/cr01386>.
- Kamruzzaman, M., Shahid, S., Islam, A., Hwang, S., Cho, J., Zaman, M., Uz, A., Ahmed, M., Rahman, M., and Hossain, M. (2021) Comparison of CMIP6 and CMIP5 model performance in simulating historical precipitation and temperature in Bangladesh: a preliminary study. *Theoretical and Applied Climatology*, 145(3), 1385–1406.
- Karl, T.R., Nicholls, N. and Ghazi, A. (1999) Clivar/GCOS/WMO workshop on indices and indicators for climate extremes workshop summary. In: *Weather and Climate Extremes*. Dordrecht, Netherlands: Springer, pp. 3–7. https://doi.org/10.1007/978-94-015-9265-9_2.
- Kim, I.-W., Oh, J., Woo, S. and Kripalani, R. (2019) Evaluation of precipitation extremes over the Asian domain: observation and modelling studies. *Climate Dynamics*, 52(3), 1317–1342. <https://doi.org/10.1007/s00382-018-4193-4>.
- Klein Tank, A.M.G., Zwiers, F.W. and Zhang, X. (2009) *Guidelines on Analysis of Extremes in a Changing Climate in Support of Informed Decisions for Adaptation*. Geneva: World Meteorological Organization. WCDMP No. 72. WMO-TD No. 1500, p. 56.
- Lavers, D.A., Harrigan, S. and Prudhomme, C. (2021) Precipitation biases in the ECMWF integrated forecasting system. *Journal of Hydrometeorology*, 22(5), 1187–1198. <https://doi.org/10.1175/JHM-D-20-0308.1>.
- Li, Z., Yu, W., Li, T., Murty, V. and Tangang, F. (2013) Bimodal character of cyclone climatology in the Bay of Bengal modulated by monsoon seasonal cycle. *Journal of Climate*, 26(3), 1033–1046. <https://doi.org/10.1175/JCLI-D-11-00627.1>.
- Limsakul, A. and Singhruck, P. (2016) Long-term trends and variability of total and extreme precipitation in Thailand. *Atmospheric Research*, 169, 301–317. <https://doi.org/10.1016/j.atmosres.2015.10.015>.
- Lubis, S.W. and Respati, M.R. (2021) Impacts of convectively coupled equatorial waves on rainfall extremes in Java, Indonesia. *International Journal of Climatology*, 41(4), 2418–2440. <https://doi.org/10.1002/joc.6967>.
- Luu, L.N., Scussolini, P., Kew, S., Philip, S., Hariadi, M.H., Vautard, R., Mai, K.V., Vu, T.V., Truong, K.B., Otto, F., van der Schrier, G., van Aalst, M.K. and van Oldenborgh, G.J. (2021) Attribution of typhoons-induced torrential precipitation in Central Vietnam, October 2020. *Climatic Change*, 169, 24.
- Marjuki, van der Schrier, G., Klein Tank, A.M.G., van den Besselaar, E.J., Nurhayati and Swarinoto, Y. (2016) Observed trends and variability in climate indices relevant for crop yields in Southeast Asia. *Journal of Climate*, 29(7), 2651–2669. <https://doi.org/10.1175/JCLI-D-14-00574.1>.
- Misra, V. and DiNapoli, S. (2014) The variability of the Southeast Asian summer monsoon. *International Journal of Climatology*, 34(3), 893–901.
- Moron, V., Robertson, A.W. and Boer, R. (2009) Spatial coherence and seasonal predictability of monsoon onset over Indonesia. *Journal of Climate*, 22(3), 840–850. <https://doi.org/10.1175/2008JCLI2435.1>.
- Moura Cardoso do Vale, T., Helena Constantino Spyrides, M., De Melo Barbosa Andrade, L., Guedes Bezerra, B. and Evangelista da Silva, P. (2020) Subsistence agriculture productivity and climate extreme events. *Atmosphere*, 11(12), 1287. <https://doi.org/10.3390/atmos11121287>.
- Muhammad, F.R., Lubis, S.W. and Setiawan, S. (2021) Impacts of the Madden–Julian oscillation on precipitation extremes in Indonesia. *International Journal of Climatology*, 41(3), 1970–1984. <https://doi.org/10.1002/joc.6941>.
- Müller, W.A., Jungclaus, J.H., Mauritsen, T., Baehr, J., Bittner, M., Budich, R., Bunzel, F., Esch, M., Ghosh, R., Haak, H., Ilmarinen, T., Klebe, T., Kornblüeh, L., Li, H., Modali, K., Notz, D., Pohlmann, H., Roeckner, E., Stemmler, I., Tian, F. and Marotzke, J. (2018) A higher-resolution version of the Max Planck Institute Earth System Model (MPI-ESM1.2-HR). *Journal of Advances in Modeling Earth Systems*, 10(7), 1383–1413.
- Ngo-Duc, T., Tangang, F.T., Santisirisomboon, J., Cruz, F., Trinh-Tuan, L., Nguyen-Xuan, T., Phan-Van, T., Juneng, L., Narisma, G., Singhruck, P., Gunawan, D. and Aldrian, E. (2017) Performance evaluation of RegCM4 in simulating extreme rainfall and temperature indices over the CORDEX-Southeast Asia region. *International Journal of Climatology*, 37(3), 1634–1647. <https://doi.org/10.1002/joc.4803>.
- Nguyen, P.-L., Bador, M., Alexander, L.V., Lane, T.P. and Ngo-Duc, T. (2022) More intense daily precipitation in cordex-sea regional climate models than their forcing global climate models over southeast asia. *International Journal of Climatology*, 42, 6537–6561. <https://doi.org/10.1002/joc.7619>.

- Nguyen-Thi, H.A., Matsumoto, J., Ngo-Duc, T. and Endo, N. (2012) A climatological study of tropical cyclone rainfall in Vietnam. *Solaiat*, 8, 41–44.
- Nguyen-Thi, T., Ngo-Duc, T., Tangang, F.T., Cruz, F., Juneng, L., Santisirisomboon, J., Aldrian, E., Phan-Van, T. and Narisma, G. (2021) Climate analogue and future appearance of novel climate in Southeast Asia. *International Journal of Climatology*, 41, E392–E409. <https://doi.org/10.1002/joc.6693>.
- Park, D.-S.R., Kim, H.-S., Kwon, M., Byun, Y.-H., Kim, M.-K., Chung, I.-U., Park, J.-S. and Min, S.-K. (2021) A performance evaluation of potential intensity over the tropical cyclone passage to South Korea simulated by CMIP5 and CMIP6 models. *Atmosphere*, 12(9), 1214. <https://doi.org/10.3390/atmos12091214>.
- Räaisaänen, J. (2007) How reliable are climate models? *Tellus A: Dynamic Meteorology and Oceanography*, 59(1), 2–29. <https://doi.org/10.1111/j.1600-0870.2006.00211.x>.
- Räsänen, T.A., Lindgren, V., Guillaume, J.H., Buckley, B.M. and Kummu, M. (2016) On the spatial and temporal variability of ENSO precipitation and drought teleconnection in mainland Southeast Asia. *Climate of the Past*, 12(9), 1889–1905. <https://doi.org/10.5194/cp-12-1889-2016>.
- Ratri, D.N., Whan, K. and Schmeits, M. (2019) A comparative verification of raw and bias-corrected ECMWF seasonal ensemble precipitation reforecasts in Java (Indonesia). *Journal of Applied Meteorology and Climatology*, 58(8), 1709–1723.
- Ratri, D.N., Whan, K. and Schmeits, M. (2021) Calibration of ECMWF seasonal ensemble precipitation reforecasts in Java (Indonesia) using bias-corrected precipitation and climate indices. *Weather and Forecasting*, 36(4), 1375–1386.
- Rauscher, S.A., Coppola, E., Piani, C. and Giorgi, F. (2010) Resolution effects on regional climate model simulations of seasonal precipitation over Europe. *Climate Dynamics*, 35(4), 685–711.
- Roberts, C.D., Senan, R., Molteni, F., Boussetta, S., Mayer, M. and Keeley, S.P. (2018) Climate model configurations of the ECMWF Integrated Forecasting System (ECMWF-IFS cycle 43r1) for HighResMIP. *Geoscientific Model Development*, 11(9), 3681–3712. <https://doi.org/10.5194/gmd-2018-90>.
- Roberts, M.J., Baker, A., Blockley, E.W., Calvert, D., Coward, A., Hewitt, H.T., Jackson, L.C., Kuhlbrodt, T., Mathiot, P., Roberts, C.D., Schiemann, R., Seddon, J., Vannière, B. and Vidale, P.L. (2019) Description of the resolution hierarchy of the global coupled HadGEM3-GC3.1 model as used in CMIP6 HighResMIP experiments. *Geoscientific Model Development*, 12(12), 4999. [10.5194/gmd-12-4999-2019-5028](https://doi.org/10.5194/gmd-12-4999-2019-5028).
- Roberts, M.J., Camp, J., Seddon, J., Vidale, P.L., Hodges, K., Vannière, B., Mecking, J., Haarsma, R., Bellucci, A., Scoccimarro, E., Caron, L.P., Chauvin, F., Terray, L., Valcke, S., Moine, M.P., Putrasahan, D., Roberts, C.D., Senan, R., Zarzycki, C., Ullrich, P., Yamada, Y., Mizuta, R., Kodama, C., Fu, D., Zhang, Q., Danabasoglu, G., Rosenbloom, N., Wang, H. and Wu, L. (2020) Projected future changes in tropical cyclones using the CMIP6 HighResMIP multimodel ensemble. *Geophysical Research Letters*, 47(14), e2020GL088662.
- Schulzweida, U., Kornblueh, L. and Quast, R. (2006) CDO user's guide. *Climate Data Operators, Version*, 1(6), 205–209.
- Schulzweida, U. and Quast, R. (2015). *Climate indices with CDO*. Available at: https://earth.bsc.es/gitlab/ces/cdo/raw/b4f0edf2d5c87630ed4c5ddee5a4992e3e08b06a/doc/cdo_eca.pdf.
- Singh, V. and Xiaosheng, Q. (2019) Data assimilation for constructing long-term gridded daily rainfall time series over Southeast Asia. *Climate Dynamics*, 53(5), 3289–3313.
- Siswanto, S., van Oldenborgh, G.J., van der Schrier, G., Jilderda, R. and van den Hurk, B. (2016) Temperature, extreme precipitation, and diurnal rainfall changes in the urbanized Jakarta city during the past 130 years. *International Journal of Climatology*, 36(9), 3207–3225. <https://doi.org/10.1002/joc.4548>.
- Sivakumar, M. (1988) Predicting rainy season potential from the onset of rains in southern Sahelian and Sudanian climatic zones of West Africa. *Agricultural and Forest Meteorology*, 42(4), 295–305.
- Skamarock, W.C., Klemp, J.B., Dudhia, J., Gill, D.O., Barker, D.M., Duda, M.G., Yu Huang, X., Wang, W. and Powers, J.G. (2008) *A description of the Advanced Research WRF version 3*. Boulder, CO: NCAR. Technical Note NCAR/TN-475+STR.
- Supari, F.T., Juneng, L., Faye, C., Jing Xiang, C., Sheau Tieh, N., Ester, S., Mohd, S.F.M., Jerasorn, S., Patama, S., Tan, P., Ngo-Duc, T., Gemma, N., Edwin, A., Dodo, G. and Ardhasena, S. (2020) Multi-model projections of precipitation extremes in Southeast Asia based on CORDEX-Southeast Asia simulations. *Environmental Research*, 184, 109350. <https://doi.org/10.1016/j.envres.2020.109350>.
- Supari, F.T., Salimun, E., Aldrian, E., Sopaheluwakan, A., and Juneng, L. (2018) ENSO modulation of seasonal rainfall and extremes in Indonesia. *Climate Dynamics*, 51(7), 2559–2580. <https://doi.org/10.1007/s00382-017-4028-8>.
- Supari, T.F., Juneng, L. and Aldrian, E. (2016) Spatio-temporal characteristics of temperature and precipitation extremes in Indonesian Bornea. *AIP Conference Proceedings*, 1784, 060050. <https://doi.org/10.1063/1.4966888>.
- Tangang, F., Chung, J.X., Juneng, L., Supari, S.E., Ngai, S.T., Jamaluddin, A.F., Mohd, M.F.S., Cruz, F., Narisma, G., Santisirisomboon, J., Ngo-Duc, T., Tan, P.V., Singhruck, P., Gunawan, D., Aldrian, E., Sopaheluwakan, A., Grigory, N., Remedio, A.R.C., Sein, D.V., Hein-Griggs, D., McGregor, J.L., Yang, H., Sasaki, H. and Kumar, P. (2020) Projected future changes in rainfall in Southeast Asia based on CORDEX-SEA multi-model simulations. *Climate Dynamics*, 55, 1247–1267. <https://doi.org/10.1007/s00382-020-05322-2>.
- Tangang, F., Supari, S., Chung, J.X., Cruz, F., Salimun, E., Ngai, S.T., Juneng, L., Santisirisomboon, J., Santisirisomboon, J., Ngo-Duc, T., Phan-Van, T., Narisma, G., Singhruck, P., Gunawan, D., Aldrian, E., Sopaheluwakan, A., Nikulin, G., Yang, H., Remedio, A.R.C., Sein, D., and Hein-Griggs, D. (2018) Future changes in annual precipitation extremes over Southeast Asia under global warming of 2°C. *APN Science Bulletin*, 8(1), 3–8. <https://doi.org/10.30852/sb.2018.436>.
- Taylor, K.E. (2001) Summarizing multiple aspects of model performance in a single diagram. *Journal of Geophysical Research: Atmospheres*, 106(D7), 7183–7192. <https://doi.org/10.1029/2000JD900719>.
- Trinh-Tuan, L., Matsumoto, J., Tangang, F. T., Juneng, L., Cruz, F., Narisma, G., Santisirisomboon, J., Phan-Van, T., Gunawan, D., Aldrian, E., and Ngo-Duc, T. (2019). Application of quantile mapping bias correction for mid-future precipitation projections over Vietnam. *SOLA* 15, 1–6
- Trouet, V. and Van Oldenborgh, G.J. (2013) KNMI Climate Explorer: a web-based research tool for high-resolution paleoclimatology. *Tree-Ring Research*, 69(1), 3–13. <https://doi.org/10.3959/1536-1098-69.1.3>.

- Ul Hasson, S., Pascale, S., Lucarini, V. and Böhner, J. (2016) Seasonal cycle of precipitation over major river basins in South and Southeast Asia: a review of the CMIP5 climate models data for present climate and future climate projections. *Atmospheric Research*, 180, 42–63. <https://doi.org/10.1016/j.atmosres.2016.05.008>.
- Van Den Besselaar, E. J., Klein Tank, A. M., Van Der Schrier, G., Abass, M. S., Baddour, O., Van Engelen, A. F., Freire, A., Hechler, P., Laksono, B. I., Jilderda, R., , Foamouhoue, A. K., Kattenberg, A., Leander, R., Güingla, R. M., Mhanda, A. S., Nieto, J. J., Sunaryo, SA., Swarinoto, Y. S., and Verver, G. (2015). International climate assessment & dataset: climate services across borders. *Bulletin of the American Meteorological Society*, 96(1):16–21.
- Van den Besselaar, E.J., Van der Schrier, G., Cornes, R.C., Iqbal, A. S. and Klein Tank, A.M. (2017) SA-OBS: a daily gridded surface temperature and precipitation dataset for Southeast Asia. *Journal of Climate*, 30(14), 5151–5165. <https://doi.org/10.1175/JCLI-D-16-0575.1>.
- Voldoire, A., Saint-Martin, D., Sénési, S., Decharme, B., Alias, A., Chevallier, M., Colin, J., Guérémy, J.-F., Michou, M., Moine, M.-P., Nabat, P., Roehrig, R., Salas y Méliá, D., Sférian, R., Valcke, S., Beau, I., Belamari, S., Berthet, S., Cassou, C., Cattiaux, J., Deshayes, J., Douville, H., Ethé, C., Franchistéguy, L., Geoffroy, O., Lévy, C., Madec, G., Meurdesoif, Y., Msadek, R., Ribes, A., Sanchez-Gomez, E., Terray, L. and Waldman, R. (2019) Evaluation of CMIP6 DECK experiments with CNRM-CM6-1. *Journal of Advances in Modeling Earth Systems*, 11(7), 2177–2213. <https://doi.org/10.1029/2019MS001683>.
- Wang, B. (2006) *The Asian Monsoon*. Berlin-Heidelberg: Springer Science & Business Media.
- WMO. (2021) *Weather-related disasters increase over past 50 years, causing more damage but fewer deaths [Press Release]*. Available at: <https://public.wmo.int/en/media/press-release/weather-related-disasters-increase-over-past-50-years-causing-more-damage-fewer>.
- Yang, H. (2012). *Revision of climate change by dynamic downscaling over the maritime continents*. Available at: adss.apcc21.org/DataSet/Cordex/CORDEX-SEA_25km.pdf [Accessed on 22nd June 2020].
- Yatagai, A., Kamiguchi, K., Arakawa, O., Hamada, A., Yasutomi, N. and Kitoh, A. (2012) APHRODITE: constructing a long-term daily gridded precipitation dataset for Asia based on a dense network of rain gauges. *Bulletin of the American Meteorological Society*, 93(9), 1401–1415. <https://doi.org/10.1175/BAMS-D-11-00122.1>.
- You, Y. and Ting, M. (2021) Low pressure systems and extreme precipitation in Southeast and East Asian monsoon regions. *Journal of Climate*, 34(3), 1147–1162. <https://doi.org/10.1175/JCLI-D-20-0206.1>.
- Zhang, L., Chen, Z., and Zhou, T. (2021). Human influence on the increasing drought risk over Southeast Asian monsoon region. *Geophysical Research Letters*, 48(11):e2021GL093777. doi : 10.1029/2021GL093777.

SUPPORTING INFORMATION

Additional supporting information can be found online in the Supporting Information section at the end of this article.

How to cite this article: Hariadi, M. H., van der Schrier, G., Steeneveld, G.-J., Ratri, D. N., Sopaheluwakan, A., Tank, A. K., Aldrian, E., Gunawan, D., Moine, M.-P., Bellucci, A., Senan, R., Tourigny, E., Putrasahan, D. A., & Linarka, U. A. (2022). Evaluation of extreme precipitation over Southeast Asia in the Coupled Model Intercomparison Project Phase 5 regional climate model results and HighResMIP global climate models. *International Journal of Climatology*, 1–21. <https://doi.org/10.1002/joc.7938>